Solid-phase synthesis of cereblon-recruiting selective histone deacetylase 6 degraders (HDAC6 PROTACs) with anti-leukemic activity

Laura Sinatra,[a#] Jing Yang,[b,c#] Julian Schliehe-Diecks,[b] Niklas Dienstbier,[b] Melina Vogt,[b] Philip Gebing,[b] Luisa M. Bachmann,[a] Melf Sönnichsen,[b] Thomas Lenz[d], Kai Stühler[e], Andrea Schöler,[a] Arndt Borkhardt,[b] Sanil Bhatia *[b] and Finn K. Hansen*[f]

[a]Institute for Drug Discovery, Medical Faculty, Leipzig University, Brüderstr. 34, 04103 Leipzig, Germany.

[b]Department of Pediatric Oncology, Hematology and Clinical Immunology, Medical Faculty, Heinrich Heine University Düsseldorf, Moorenstr. 5, 40225 Düsseldorf, Germany.

[c]Department of Medicine, Yangzhou Polytechnic College, West Wenchang Road 458, Yangzhou, 225009, P.R. China.

[d]Molecular Proteomics Laboratory, Biological Medical Research Center, Heinrich-Heine-University Düsseldorf, Universitätsstr. 1, 40225 Düsseldorf, Germany.

[e]Institute for Molecular Medicine, Proteome Research, University Hospital and Medical Faculty, Heinrich-Heine-University Düsseldorf, Universitätsstr. 1, 40225 Düsseldorf, Germany.

[f]Pharmaceutical Institute, Department of Pharmaceutical and Cell Biological Chemistry, University of Bonn, An der Immenburg 4, 53121 Bonn, Germany.

Abstract

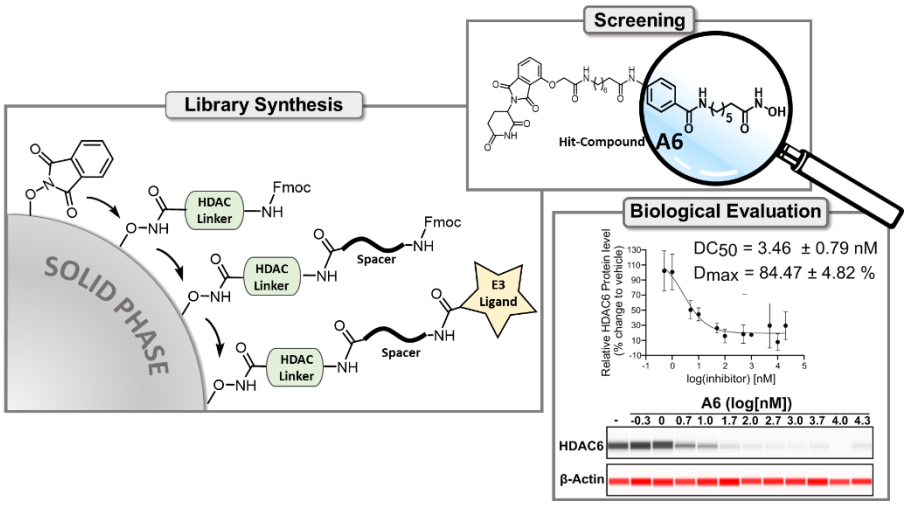

In this work, we utilized the proteolysis targeting chimera (PROTAC) technology to achieve the chemical knock-down of histone deacetylase 6 (HDAC6). Two series of cereblon-recruiting PROTACs were synthesized via a solid-phase parallel synthesis approach, which allowed the rapid preparation of two HDAC6 degrader mini libraries. The PROTACs were either based on an unselective vorinostat-like HDAC ligand or derived from a selective HDAC6 inhibitor. Notably, both PROTAC series demonstrated selective degradation of HDAC6 in leukemia cell lines. The best degraders from each series (denoted **A6** and **B4**) were capable of degrading HDAC6 via ternary complex formation and the ubiquitin−proteasome pathway, with DC_{50} values of 3.5 and 19.4 nM, respectively. PROTAC **A6** demonstrated promising antiproliferative activity via inducing apoptosis in myeloid leukemia cell lines. These findings highlight the potential of this series of degraders as effective pharmacological tools for the targeted degradation of HDAC6.

Introduction

The emerging technology of **pro**teolysis **ta**rgeting **c**himeras (PROTACs) opens new paths to modulate and study proteins for potential therapeutic approaches. PROTACs are molecules of bifunctional nature, incorporating two ligands, one for E3 ubiquitin ligase binding and one for the protein of interest (POI) binding, connected through a linker with variable length and chemical properties.[1–3] Once the chimeric molecule binds to the E3 ligase and the POI, an E3 ligase:PROTAC:POI ternary complex is formed, thereby inducing polyubiquitination of the POI and its subsequent degradation via the proteasome (Figure 1A). In recent years many efforts have been undertaken to drug new targets by targeted protein degradation and to develop new E3 ligase recruiting ligands.[4–6] In 2019, the first PROTAC entered clinical trials and the most advanced PROTACs bavdegalutamide (ARV-110, an androgen receptor degrader) and ARV-471 (an estrogen receptor degrader) have already reached phase II trials and showed promising early data in terms of tolerability, safety and efficacy.[7,8] More than 10 targeted protein degraders have reached the clinic by the end of 2021[9] which underscores the vast potential of PROTACs and other targeted protein degraders as new therapeutic modalities.

Histone deacetylases (HDACs) are key players in the epigenetic network regulating the transcription of numerous proteins and many processes by removing acetyl and other acyl groups from histones as well as non-histone proteins.[10,11] To date, 18 human HDAC isoforms have been identified: The Zn^{2+}-dependent HDACs, subdivided into three classes, including class I (HDAC 1, 2, 3, 8), II (class IIa: HDAC4, 5, 7, 9; class IIb: HDAC6, 10) and IV (HDAC11) and the NAD^{+}-dependent class III enzymes (sirtuins 1-7).[12] Class I HDACs, mostly localized in the nucleus, are ubiquitously expressed and play a crucial role in cell survival and proliferation, whereas class II HDACs are expressed more tissue specific and can shuttle between the nucleus and cytoplasm.[13] An overexpression of HDACs is linked to various diseases including solid and hematological malignancies.[14] The efficacy of HDAC inhibitors (HDACi), especially of non-selective inhibitors, as anticancer agents has been widely proved.[15–18] However, pan-HDACi often possess serious adverse effects. Consequently, the development of selective HDACi, particularly HDAC6 selective inhibitors, is increasingly of interest to optimize the risk-benefit profile of HDACi.[19] However, besides the crucial catalytic functions mediated via the HDAC6 second catalytic domain (CD2), HDAC6 can also influence cellular processes via the more enigmatic first catalytic domain (CD1) and the unique zinc-finger ubiquitin binding domain (ZnF-UBP), which both are not inhibited by classical HDAC6 selective inhibitors.[20,21] Hence, the targeted degradation of HDAC6 may

be advantageous over the well-established selective HDAC6 CD2 inhibition, because this approach eliminates both catalytic domains as well as the ubiquitin binding domain.[20]

The development of HDAC degraders is of emerging interest and a few HDAC degraders were disclosed in recent years.[22–37] In 2017, Schiedel *et al.* described the first degraders of sirtuin 2 (Sirt2).[22] The first degraders of a Zn^{2+}-dependent HDAC were reported in 2018 by Yang *et al.* by utilizing pomalidomide as a recruiter for the E3 ligase cereblon (CRBN) and the unselective HDACi crebinostat as POI ligand.[23] Somewhat surprisingly, despite the unselective HDACi scaffold, the PROTACs achieved selective degradation of HDAC6. Subsequently, additional selective HDAC6 degraders were discovered based on the selective HDAC6i nexturastat A.[30–33,35] These findings raise the intriguing question, whether a selective or unselective HDAC6 ligand is superior to develop highly efficient and selective HDAC6 degraders. Even though most work on HDAC PROTACs has focused on HDAC6,[38] the first degraders of HDAC1, HDAC2, and/or HDAC3 utilizing a hydrazide or aminoanilide zinc-binding group were recently disclosed.[24,28,36,37] Furthermore, in 2022, the first selective HDAC4[39] and HDAC8[27,29,40] PROTACs were reported. Interestingly, a chemo-proteomics study by Xiong *et al.* demonstrated that HDAC6 and HDAC3 are most amenable for targeted protein degradation.[26]

Degradation efficiency of PROTACs depends on multiple factors. One critical factor is the formation of the ternary complex, which still remains empirical and difficult to predict by rational design.[41] Thus, efficient synthesis protocols allowing the rapid synthesis of different PROTACs with altered linker types and E3 ligase as well as POI ligands are an urgent need for hit optimization. Here we report a facile and straightforward synthetic gateway towards HDAC6 PROTACs using a combination of solution- and solid-phase chemistry. The synthesized PROTACs induced significant and selective degradation of HDAC6 in leukemia cells. The degradation efficiency and kinetics of the most promising degraders were further analyzed by automated capillary western blot, fluorescence microscopy, and endogenously tagged HiBiT-HDAC6 K562 cells. The biological evaluation of the best degrader included viability, apoptosis, and caspase 3/7 assays as well as cell cycle analysis.

Results and discussion

Design and synthesis of HDAC6 degraders. In order to investigate whether a selective or an unselective HDAC ligand is superior for efficient and selective HDAC6 degradation, we designed two series of HDAC6 degraders. In the first series (**A1-6**), we utilized a vorinostat-like HDAC ligand based on an alkyl linker. In the second series (**B1-4**), we choose a selective benzimidazole-based HDAC6

ligand, which was derived from a selective HDAC6i reported by Shen *et al.*[42] For HDAC6i building block synthesis (Figure 1B), 2-methyl-6-nitro-1*H*-benzo[*d*]imidazole (**1**) was alkylated with methyl 4-(bromomethyl)-3-fluorobenzoate (**2**) yielding the intermediate **3**, which was separated from its minor regioisomer featuring the nitro group in 6-position. The major isomer **3** was further treated in a reaction sequence including reduction of the nitro group, saponification of the ester and Fmoc-protection without any purification steps in between to afford the Fmoc-protected building block **4**.

The designed PROTACs were synthesized following our previously published approach using hydroxamic acids immobilized on resins (HAIRs).[43] In detail, the preloaded resins were prepared by immobilization of hydroxylamine on commercially available 2-chlorotrityl chloride (2-CTC) resin, followed by coupling of the Fmoc-protected HDACi moieties. The synthesis of the first series (**A1-6**) was completely carried out on resin. To this end, the readily available phthaloyl-protected resin **5** was deprotected by treatment with hydrazine hydrate followed by an amide coupling

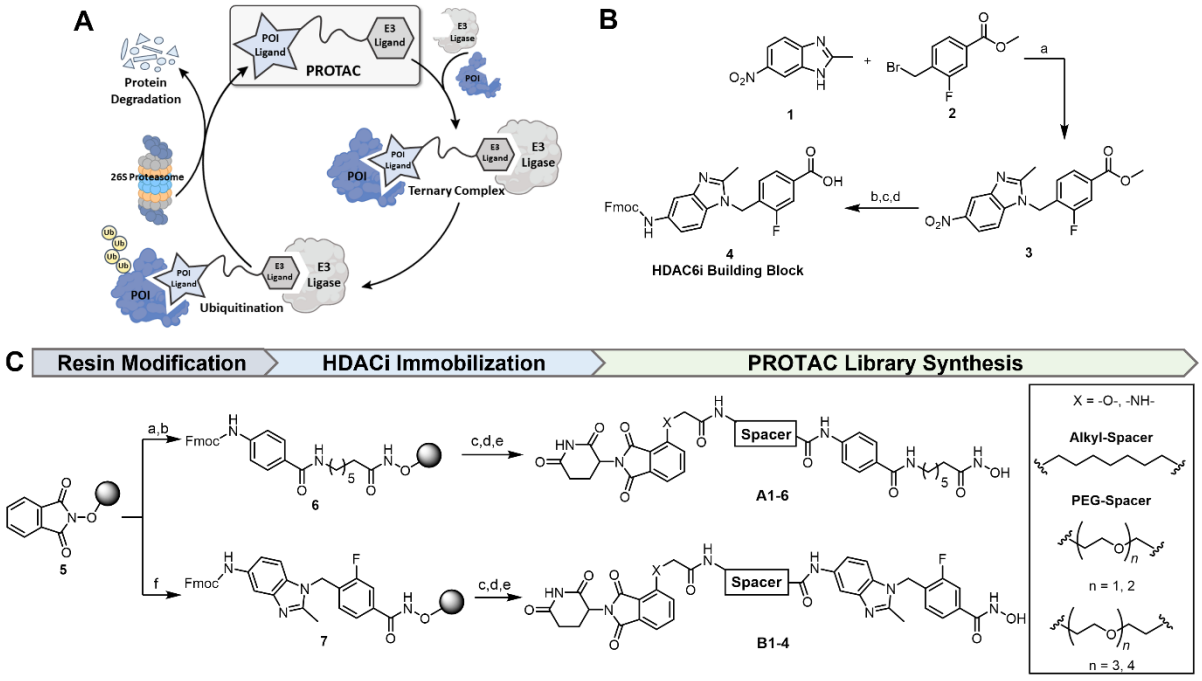

Figure 1: A. Schematic representation of the POI degradation mediated by a PROTAC. **B.** Solution phase synthesis of the HDAC6i building block **4**: a.) Cs_2CO_3 (2.0 equiv.), THF, 80 °C, 2 h, 44%. b.) H_2, 10% Pd/C, MeOH/CH_2Cl_2 (5:1), r.t., 4 h. c.) $NaOH_{aq}$ (4.0 equiv.), THF/MeOH (5:1), r.t., 2 h. d.) Fmoc-Cl (1.5 equiv.), 5 % $Na_2CO_{3\ aq}$/1,4-dioxane (3:2), 0 °C to r.t., 18 h, 82% over 3 steps. **C.** Solid-phase synthesis of the first (**A1-6**) and second (**B1-4**) series of PROTACs, a.) i. 5% $N_2H_4 \cdot H_2O$ in MeOH, r.t., 2 x 15 min, ii. Fmoc-7-aminoheptanoic acid (2.0 equiv.) HATU (2.0 equiv.), HOBt·H_2O (2.0 equiv.), DIPEA (3.0 equiv.) DMF, r.t., 20 h., loading determined: 0.77 - 0.97 mmol/g. b.) i. 20% piperidine, DMF, 2 x 5 min, ii. Fmoc-4-aminobenzoic acid (3.0 equiv.), HATU (3.0 equiv.), DIPEA (4.0 equiv.), DMF, r.t., 20 h. c.) i. 20% piperidine, DMF, 2 x 5 min, ii. Fmoc-spacer-COOH (3.0 equiv.), HATU (3.0 equiv.), DIPEA (4.0 equiv.), DMF, r.t. 4 h. d.) i. 20% piperidine, DMF, 2 x 5 min, ii. Thalidomide-X-CH_2COOH building block (2.0 equiv.), HATU (2.2 equiv.), DIPEA (3.5 equiv.), DMF, r.t., 4 h, e.) 5% TFA, CH_2Cl_2, r.t., 1 h, 27-71% over all solid-phase steps. f.) i. 5% $N_2H_4 \cdot H_2O$ in MeOH, r.t., 2 x 15 min, ii. **4** (2.0 equiv.), HATU (2.0 equiv.), HOBt·H_2O (2.0 equiv), DIPEA (3.0 equiv.), DMF, r.t., 20 h, loading determined: 0.60 - 0.62 mmol/g.

with Fmoc-7-aminoheptanoic acid. The subsequent Fmoc deprotection and amide coupling with Fmoc-4-aminobenzoic acid afforded the preloaded resin **6** (Figure 1C). In contrast, the resin-bound

benzimidazole-based HDAC6 ligand **7**, used for the synthesis of the second series of PROTACs (**B1-4**), was generated by immobilization of the previously synthesized building block **4**. Library synthesis of the desired PROTACs **A1-6** and **B1-4** was carried out starting from **6** or **7** using a solid-phase supported parallel synthesis approach. In the first step, we introduced different PEG-based linkers or 8-aminooctanoic acid as spacer moiety into both series (Figure 1C). For the E3 ligase-recruiting part, we chose the CRBN ligands hydroxythalidomide and pomalidomide, which were synthesized using modified literature known procedures, carrying an additional acetic acid residue for the following solid-phase approach.[44,45] Coupling of the E3 ligase component completed the PROTAC synthesis. The cleavage from the resin under gentle conditions generated the hydroxamic acids **A1-6** and **B1-4** in excellent crude purities of up to 91%. Before the biological evaluation, the compounds were further purified by preparative RP-HPLC to >95% purity yielding the final PROTACs in total yields of 27 - 71%. Taken together, this synthetic strategy enabled PROTAC library generation in a highly time efficient fashion.

***In vitro* HDAC inhibition assays.** The synthesized PROTACs were first screened in biochemical assays to investigate their inhibition of HDAC1 and 6. The results are summarized in Table 1. All compounds from both series demonstrated potent inhibition of HDAC6 with IC_{50} values in double- or even single-digit nanomolar concentration range. As expected, the vorinostat-like derivatives of type **A1-6** turned out to be unselective inhibitors and also showed potent inhibition of HDAC1 leading to selective indices ($SI^{1/6}$) ranging from 6 to 20. In contrast, the compounds from the benzimidazole series (**B1-4**) displayed high selectivity for HDAC6 ($SI^{1/6}$ = 100-129).

Selection and *in vitro* functional evaluation of PROTACs. In the next step, all PROTACs were analyzed regarding their potential to degrade HDAC6 in the cellular context. To this end, HL-60 leukemia cells were treated for 6 h or 24 h with different concentrations (0.1, 1, and 10 µM) of each PROTAC and subsequently investigated by western blot in regards to degradation of HDAC1 and HDAC6 as well as hyperacetylation of α-tubulin (Figure S1-4, Supporting Information). Independent of the concentration used and the incubation time, there was no change observed in the protein level of HDAC1. In contrast, all PROTACs were able to reduce the HDAC6 levels although with different efficiency. Interestingly, in both series the PROTACs containing 8-aminooctanoic acid as linker moiety (**A6** and **B4**) demonstrated the most potent degradation of HDAC6 and the strongest hyperacetylation of α-tubulin, which is a marker

Table 1: In vitro inhibition of HDAC1 and 6 by the PROTACs **A1-7** and **B1-4**.

Code	Structure	HDAC Inhibition IC_{50} [µM]		SI	Code	Structure	HDAC Inhibition IC_{50} [µM]		SI
		HDAC1	HDAC6				HDAC1	HDAC6	
A1	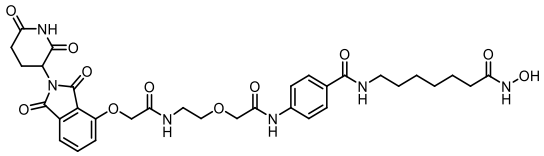	0.155 ± 0.027	0.012 ± 0.001	13	**A7**	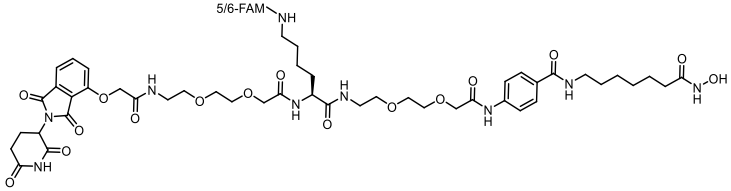	0.144 ± 0.009	0.0156 ± 0.0004	9
A2	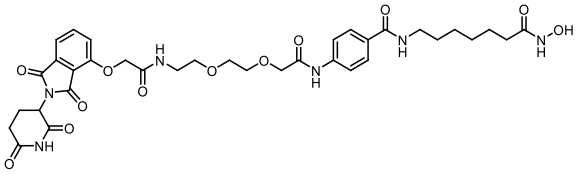	0.174 ± 0.009	0.0268 ± 0.0004	6	**B1**	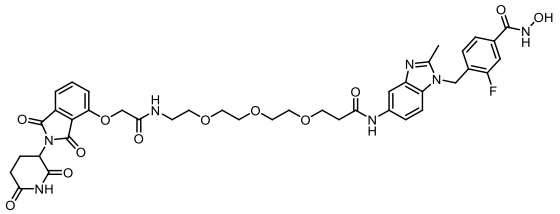	1.314 ± 0.134	0.0134 ± 0.0007	101
A3	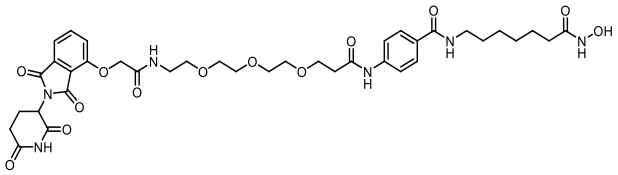	0.161 ± 0.015	0.017 ± 0.002	10	**B2**	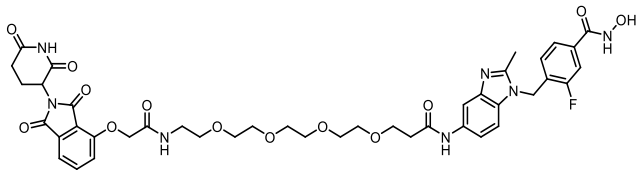	1.494 ± 0.032	0.015 ± 0.001	100
A4	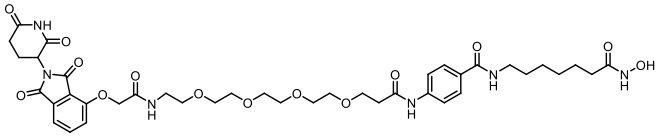	0.208 ± 0.005	0.0208 ± 0.0008	10	**B3**	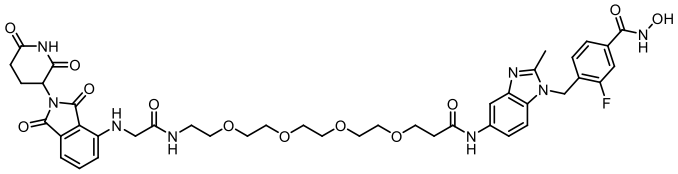	1.420 ± 0.054	0.013 ± 0.001	110
A5	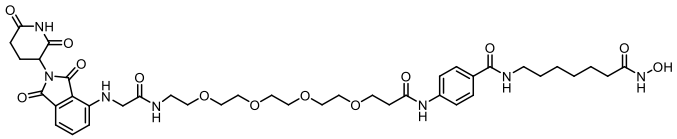	0.186 ± 0.018	0.015 ± 0.001	12	**B4**	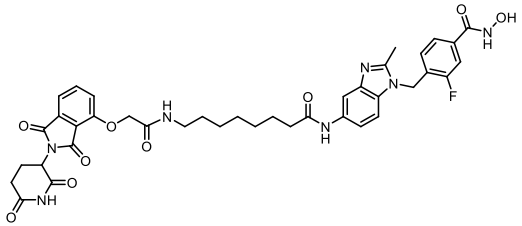	0.647 ± 0.087	0.00454 ± 0.0004	129
A6	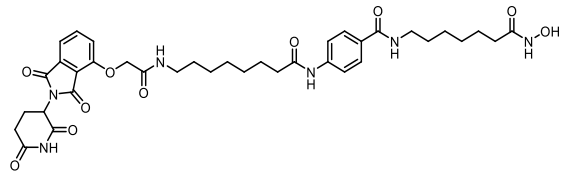	0.100 ± 0.011	0.00486 ± 0.0003	20	**SAHA**	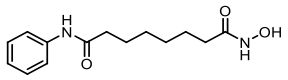	0.088 ± 0.013	0.027 ± 0.007	3

of decreased HDAC6 activity. Consequently, both degraders were selected for a detailed biological investigation (Figure 2A).

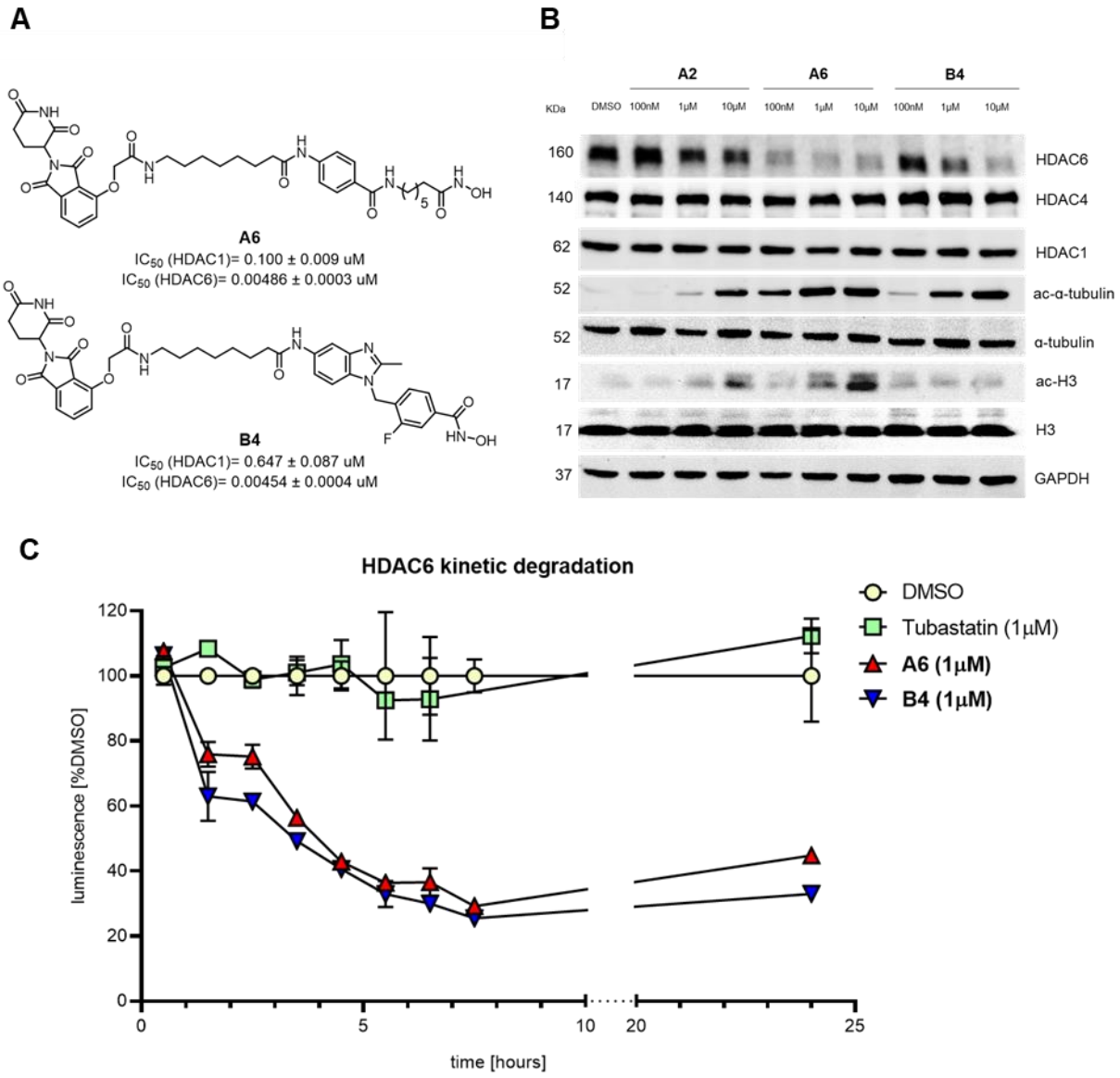

Figure 2: **A.** Structures of compounds **A6** and **B4**, which were selected for further biological evaluation. **B.** HL-60 cells were treated with 100 nM, 1 µM, 10 µM of **A2**, **A6**, **B4** for 6 h. Afterwards, cell lysates were immunoblotted with anti-HDAC6, HDAC4, HDAC1, acetyl-α-tubulin, acetyl-histone H3, total α-tubulin, and total histone H3 antibodies. GAPDH was used as a loading control. **C.** Kinetic degradation of HDAC6 levels upon incubation with **A6** or **B4** (1 µM) in HiBit tagged K562 cells, whereas tubastatin (1 µM) and DMSO served as a negative control. The luminescence was measured using Nano-Glo HiBit lytic detection system (n=3).

In the first step, we compared the degradation efficiency of **A6** with our previously published prototypic HDAC6 degrader **A2**.[43] **A2** and **A6** are identical in terms of the HDAC warhead and E3 ligase ligand as well as chain length of the PROTAC linker. However, they differ in the linker type. Western blot experiments demonstrated that the HDAC6 degradation efficiency was clearly improved when the PEG-

based linker present in **A2** (see Table S1) was replaced by the 8-aminooctanoic acid linker, as utilized in the case of **A6**. We calculated the physiochemical properties of PROTACs **A1-6** and **B1-4** using SwissADME (Table S1, Supporting Information). **A6** (log *P*: 2.37) displayed a significantly higher calculated log *P* value than **A2** (log *P*: 0.63) which makes it reasonable to assume that the improved degradation of HDAC6 arises from improved permeability due to a higher lipophilicity. When **A6** was analyzed head to head with the most potent PROTAC from the benzimidazole series (**B4**), **A6** turned out to be the slightly more efficient HDAC6 degrader (Figure 2B). Of note, no reduction of HDAC1 (as a representative class I isoform) and HDAC4 (as a representative class IIa isoform) protein levels was observed demonstrating that **A6** and **B4** are potent and selective HDAC6 PROTACs (Figure 2B). On the other hand, while both compounds were capable of inducing hyperacetylation of α-tubulin in HL-60 cells, only **A6**, but not **B4**, caused hyperacetylation of histone H3. Since **A6** did not degrade HDAC1 (Figure 2B) but displayed submicromolar inhibitory activity toward HDAC1 (IC_{50}: 0.100 µM, Table 1), we assume that the observed hyperacetylation of histone H3 originates from unselective HDAC inhibition and not from degradation. These results indicate that the selectivity for increasing the level of acetylated tubulin over acetylated histone H3 can be improved by replacing an unselective HDACi by a selective HDAC6i as the HDAC6 ligand in PROTACs. These findings are in excellent agreement with the report of Tang and co-workers who showed that PROTACs based on the pan-HDACi crebinostat caused hyperacetylation of α-tubulin and histone H3, whereas PROTACs based on the HDAC6 selective inhibitor nexturastat A demonstrated selective hyperacetylation of α-tubulin.[46] Next, we evaluated the kinetics of HDAC6 degradation by generating (endogenous) HDAC6 fused HiBit[47] K562 cells and measured the degradation efficiency after incubation with **A6** or **B4** with a luminescent based assay**.** The degradation profiles of both degraders were similar with comparable D_{max} values and the most pronounced reduction of HDAC6 levels was observed in both cases between 5.5 and 7.5 h after treatment (Figure 2C). In line, **A6** and **B4** (at 100 nM and 1000 nM) demonstrated potent HDAC6 degradation as well as hyperacetylation of α-tubulin in a multiple myeloma cell line U266, thereby confirming that the activity of these degrader is not restricted to leukemia cell lines (Figure S5, Supporting Information). Next, we performed a quantitative mass spectrometry (MS) analysis to determine the effects of PROTACs on the global cellular proteome. Overall, we found no significant changes in protein expression pattern (4331 proteins identified with two or more Razor + unique peptides) after 6 h PROTAC treatment (**A6** or **B4** at 1 µM, Figure S6A-B, Supporting Information). In line with the immunoblot analysis (Figure 2B), HDAC6 was identified only in the cells that were not

treated with the PROTACs (Table S2, Supporting Information). However, because of the small number of observations (one MS/MS count, respectively, in three of the five untreated replicates; three unique peptides in total), we omitted to perform a quantitative interpretation of HDAC6's MS data (Figure S6C and Table S3, Supporting Information). With regard to other HDAC related proteins (HDAC1-11, SIRT1-7, and HDRP), HDAC1/2/3/6/7/10 and SIRT1/2/3/5/6 were identified, of which HDAC1/2 and SIRT5 were reliably quantifiable, but were not affected by the PROTACs (Table S2, Supporting Information).

Next, the degradation efficiency of **A6** and **B4** was quantified by automated capillary western blot utilizing the simple western immunoassay technology (Figure 3A and Figure S7, Supporting Information). Both PROTACs revealed DC_{50} values for HDAC6 in the low nanomolar range and D_{max} values of over 80%. Degrader **A6** (DC_{50}: 3.5 nM) was slightly more efficient compared to **B4** (DC_{50}:19.4 nM). In addition, HDAC6 degradation was accompanied with dose-dependent α-tubulin hyperacetylation with an EC_{50} of 0.4 µM and 5.5 µM for **A6** and **B4**, respectively. Interestingly, **B4** required a higher concentration to induce α-tubulin hyperacetylation than **A6**. However, both HDAC6 inhibition and HDAC6 degradation contribute to the α-tubulin hyperacetylation. Keeping in mind that both compounds reduced HDAC6 levels to ~ 10-15%, there is still HDAC6 available which can be inhibited. Differences in the intracellular target engagement of HDAC6 by **A6** and **B4** might explain the observed differences in the α-tubulin hyperacetylation in the quantitative simple western immunoassays (Figure 3A), which were also confirmed by classical western blot experiments (Figure 2B).

Additional western blot experiments were performed to confirm that the ubiquitin−proteasome system is involved in the decrease of HDAC6 protein levels. The pretreatment of HL-60 cells with the proteasome inhibitor MG132 for 1 h followed by the addition of PROTACs **A6** or **B4** inhibited the degradation of HDAC6 (Figure 3B). Moreover, pretreatment of HL-60 cells for 1 h with either the pan-HDACi vorinostat or the selective HDAC6i nexturastat A before treatment with **A6** or **B4** also rescued HDAC6 from degradation (Figure 3B). These results indicate that the formation of the CRBN:PROTAC:HDAC6 ternary complex, which was blocked by the respective HDACi, is crucial for HDAC6 degradation. Similarly, degradation of HDAC6 was rescued by pretreatment with the CRBN ligand pomalidomide (Figure 3C). Taken together, these data demonstrate that the degradation of HDAC6 occurs via the ternary complex formation and ubiquitin−proteasome pathway.

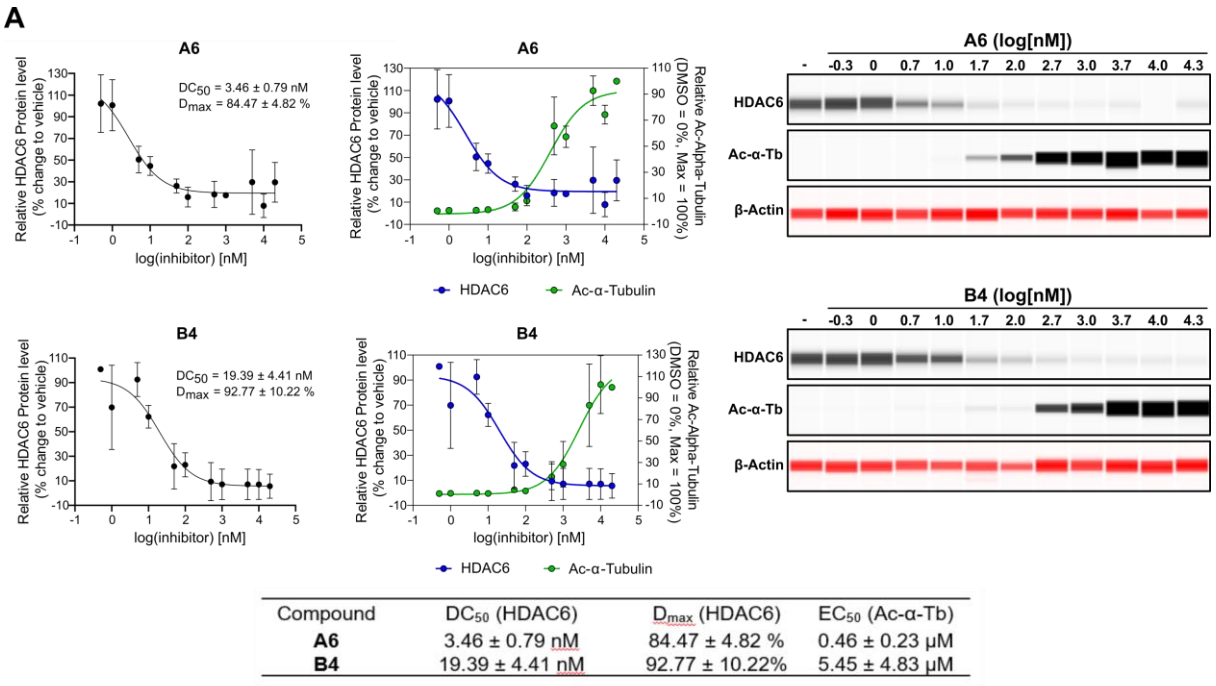

Compound	DC_{50} (HDAC6)	D_{max} (HDAC6)	EC_{50} (Ac-α-Tb)
A6	3.46 ± 0.79 nM	84.47 ± 4.82 %	0.46 ± 0.23 µM
B4	19.39 ± 4.41 nM	92.77 ± 10.22%	5.45 ± 4.83 µM

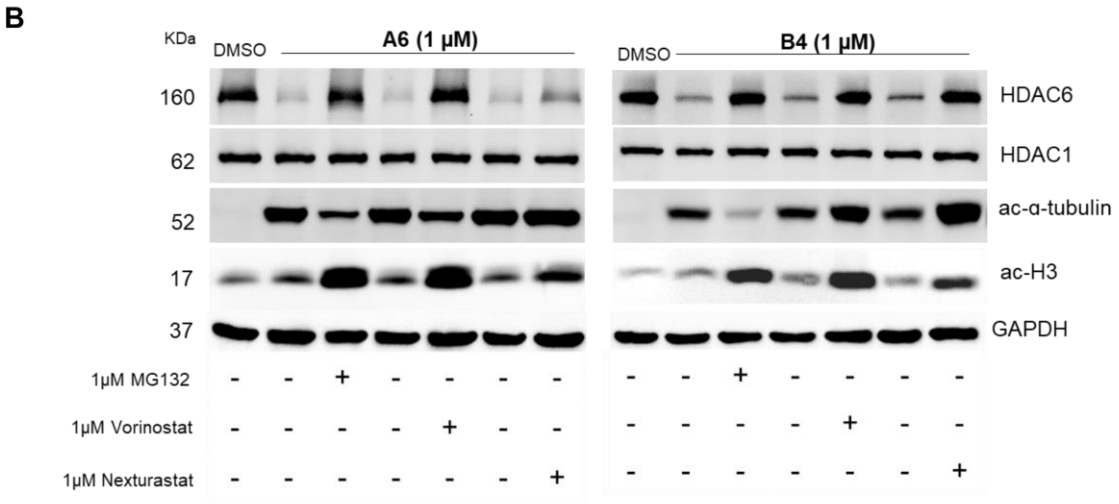

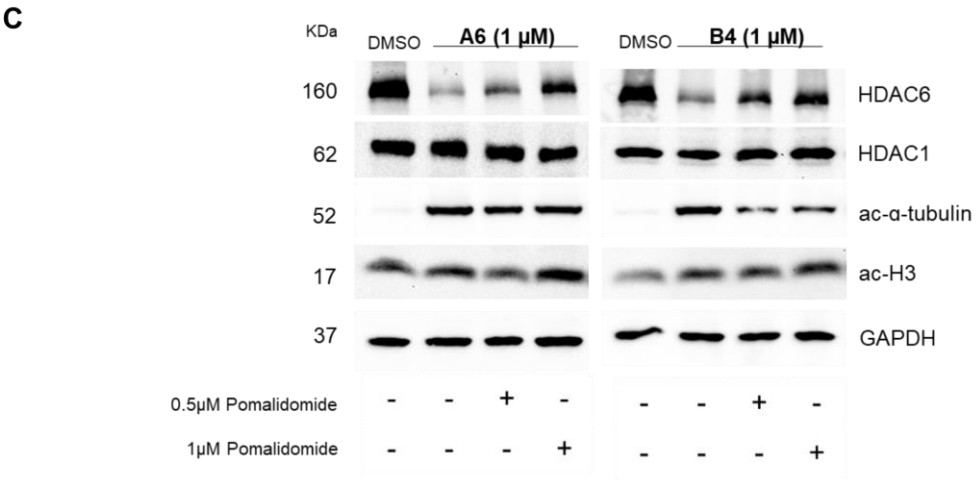

Figure 3: **A.** Quantitative simple western immunoassay shows dose-dependent degradation of HDAC6 with subsequent increased levels of acetyl-α-tubulin. HL-60 cells were treated with the indicated concentrations of **A6** or **B4** for 6 h and the resulting lysates (0.40 µg/sample) were analyzed utilizing simple western immunoassay technology (BioTechne). Samples were quantified by normalizing the area under the curve (AUC) values of the electropherogram from the vehicle control. DC_{50} and Dmax were calculated using non-linear regression (log(inhibitor) vs response (three parameters)). EC_{50} for α-tubulin hyperacetylation was

calculated using non-linear regression (log(agonist) vs normalized response – variable slope). Average DC_{50}, Dmax and EC_{50} values were calculated from three independent simple western immunoassay runs on the treated samples from two independent biological replicates. A representative immunoblot is depicted here. **B.** HL-60 cells were pretreated with vehicle (DMSO), MG132, Vorinostat or Nexturastat A (1 μM) for 1 h, followed by treatment with **A6**, **B4** (1 μM) or DMSO for 6 h. Afterwards, cell lysates were immunoblotted with anti-HDAC6, HDAC1, acetyl-α-tubulin and acetyl-histone H3 antibodies. GAPDH was used as a loading control. **C.** HL-60 cells were pretreated with Pomalidomide (0.5 μM or 1 μM) or vehicle (DMSO) for 1 h, followed by treatment with **A6**, **B4** (1 μM) or vehicle (DMSO) for 6 h. Afterwards, cell lysates were immunoblotted with anti-HDAC6, HDAC1, acetyl-α-tubulin and acetyl-histone H3 antibodies. GAPDH was used as a loading control.

Fluorescence microscopy. The degradation efficiency of the most potent degrader **A6** was further investigated by fluorescence microscopy (Figure 4). HL-60 cells were treated with either 100 nM or 1 μM of **A6** for 3 and 6 h, after which they were fixed and stained with anti-HDAC6 antibody to measure changes in HDAC6 signal intensity. We recorded z-stacks for all images with a conserved z-step size to create maximum intensity projections of each cell, which enabled us to display HDAC6 signals from the entire cell volume. Of note, acquisition settings were conserved between all the conditions. We observed that 3 h treatment with **A6** at 100 nM was sufficient to degrade HDAC6 as seen by the reduction in fluorescence intensity (Figure 4A-C). Extending the incubation period from 3 to 6 h appears to have a marginal effect on the HDAC6 signal (Figure 4A-C vs. D-F). Furthermore, smaller differences in HDAC6 signals were visible when HL-60 cells were treated with 1 μM of **A6** (i.e. 10-fold higher). In line with the western blot results, no change in the levels of HDAC1 was overserved by fluorescence microscopy after 3 or 6 h treatment with either 100 nM or 1 μM of **A6** (Figure S8, Supporting information).

Next to study the intracellular localization of our HDAC degraders, we synthesized the fluorescently tagged PROTAC **A7** (Figure S6, Supporting Information) by incorporating a fluorescein-labelled lysine in the middle of the PROTAC linker. HL-60 cells were treated with either 1, 10, or 50 nM concentrations of **A7** for 6 h. The signal intensity of HDAC6 did not change significantly when HL-60 cells were treated with 1 or 10 nM of **A7**, whereas, 50 nM of **A7** significantly reduced HDAC6 levels (Figure S6D, Supporting Information). However, the localization of HDAC6 was changed even at lower concentration of **A7** (i.e. 1, 10 and 50 nM), as the dot-like signals for HDAC6 were more detached from the nuclear-cytoplasmic interface, when compared to the DMSO control (Figure S9, Supporting Information). We also paid close attention to the localization of our fluorescent compound **A7**. However, in contrast to changes in the HDAC6 intracellular localization, the co-localization of **A7** was not detected conclusively in the nucleus (Figure S9, Supporting Information).

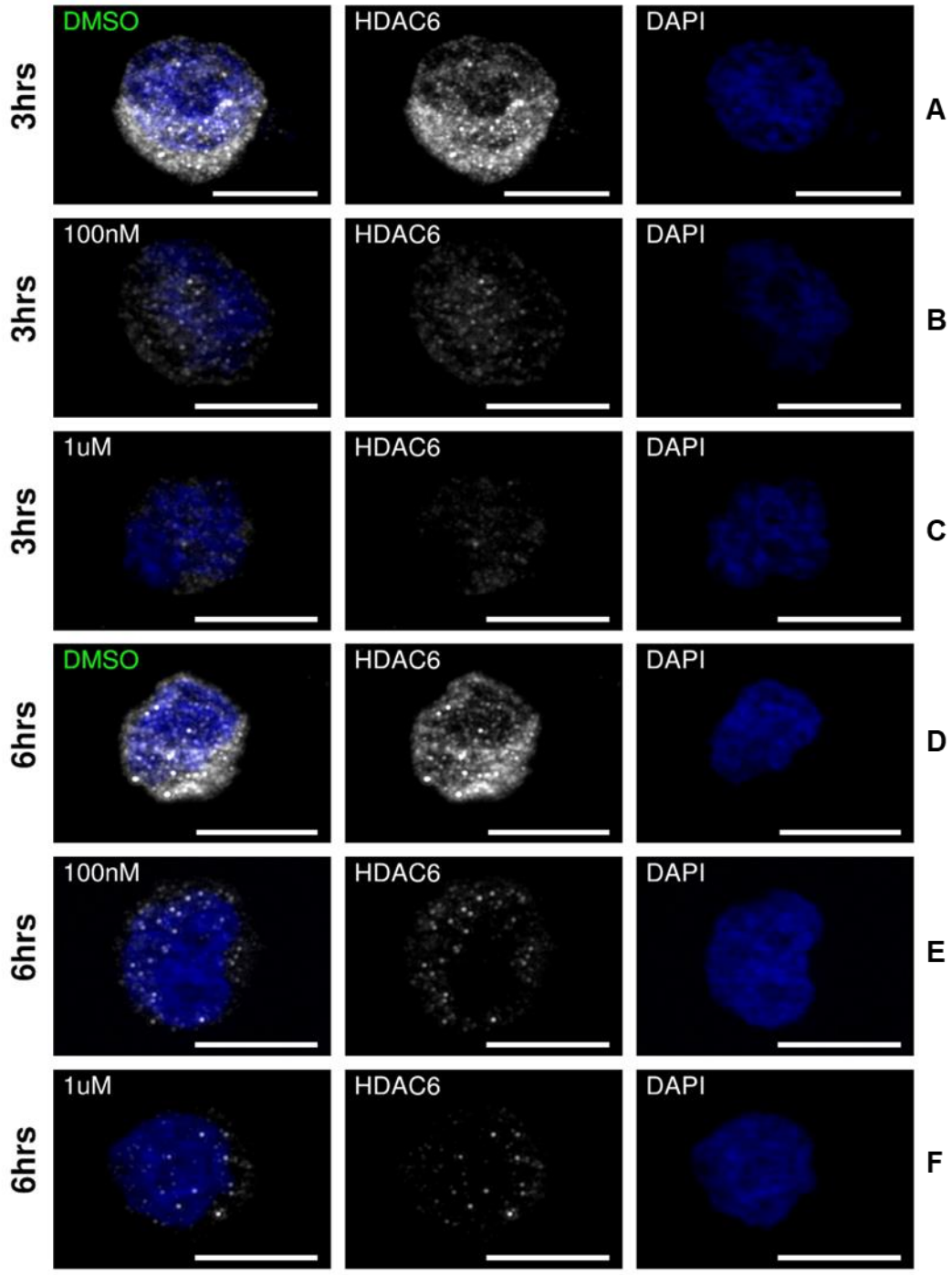

Figure 4: HDAC6 is degraded in HL-60 cells treated with 100 nM and 1 uM **A6** for 3 and 6 h. Row A/D - HL-60 cells treated control. Row B,C,E,F - HL-60 cells were treated with either 100 nM and 1 uM concentrations of **A6** for 3 or 6 h. All samples were stained with an anti-HDAC6 antibody (white), as well as DAPI nuclear stain (blue). HDAC6 is visibly reduced when treated with **A6** for both 3 and 6 h. Brightness and contrast were adjusted equally for all images. Scale bar = 10 µm.

Efficacy of A6 and B4 against leukemia cell lines. After identifying **A6** and **B4** as the lead PROTACs that effectively reduced the HDAC6 levels, we further investigated their anti-leukemic activity. At first, we investigated the effect of **A6** and **B4** exposure on the cell viability of leukemia cell lines originated from different therapy refractory subgroups of acute myeloid leukemia or AML (HL-60, Kasumi, THP-1,

HL-60, SKNO1 and MOLM13) and B-cell acute lymphoblastic leukemia or B-ALL (REH and 697), using an ATP-Glo based assay (Figure 5A, B and Table S4, Supporting Information). Exposure of **B4** did not display any inhibitory effects on the cellular viability of any tested leukemia cell line in the 0.5 - 50 µM concentration range, whereas **A6** revealed IC_{50} values in the double-digit micromolar range in three of the AML cell lines (MV4-11, SKNO-1 and MOLM13). The low effects of **B4** (a selective HDAC6 degrader and selective HDAC6 inhibitor) on the cellular viability is in agreement with recent reports that selective HDAC6 inhibitors do not show antiproliferative activities when used at selective concentrations.[48,49] The reduced cytotoxicity of **A6** (a selective HDAC6 degrader and unselective HDAC inhibitor) compared to vorinostat and nexturastat A is somewhat surprising, because its inhibitory properties against class I isoforms (similar HDAC1 inhibitory activity as vorinostat, see Table 1) should lead to more pronounced antiproliferative properties. For assessing the nuclear permeability **A6** *vs* vorinostat, HL60 cells were treated with vorinostat or **A6** at 1 µM for 24 h. Interestingly, a significantly higher H3 hyperacetylation was noticed upon incubation with vorinostat in comparison to **A6**. These results hint that the differences seen between the IC_{50} values of **A6** (double-digit micromolar) and vorinostat (sub-micromolar) likely arise due to reduced nuclear permeability of **A6** (Figure S10, Supporting Information).

Out of these three AML cell lines, **A6** displayed the lowest IC_{50} in the MOLM13 cell line (17.4 ± 3.1 µM) and therefore this cell line was selected for further validation studies, involving apoptosis induction and cell cycle progression. Exposure of MOLM13 to **A6** induced caspase 3/7 dependent apoptosis in dose dependent fashion, which was further validated by annexin V and PI staining, whereas vorinostat at its IC_{25} and IC_{50} concentration in MOLM13 cells was taken a positive control in both assays (Figure 5C, D). Next, the effect of **A6** on the cell cycle progression of MOLM13 cells was evaluated using flow cytometry (Figure 5E). Dose-dependent increase in sub-G1 fraction (DNA fragmentation as a marker of apoptosis) with a concomitant reduction of cell population in G2/M phase was reported after 48 h exposure to **A6** (8, 16 and 24 µM), whereas vorinostat was taken as a control (Figure 5E). The proportions of the cells with the fragmented DNA (sub-G1 population) in the vehicle treated group was 4.9%, which increased up to 7.5%, 9.9% and 13.4% upon treatment with 8, 16 and 24 µM of **A6**. These results specify that **A6** inhibits the cell cycle progression of MOLM13 cells, which explains the effect of **A6** exposure on cell viability and apoptosis induction.

Taken together, these results indicate that PROTAC **A6** reduces the cell viability in three AML cell lines in the double digit micromolar range and also induces apoptosis of MOLM13 cells in a caspase 3/7 dependent fashion through arresting the cells in sub-G1 phase.

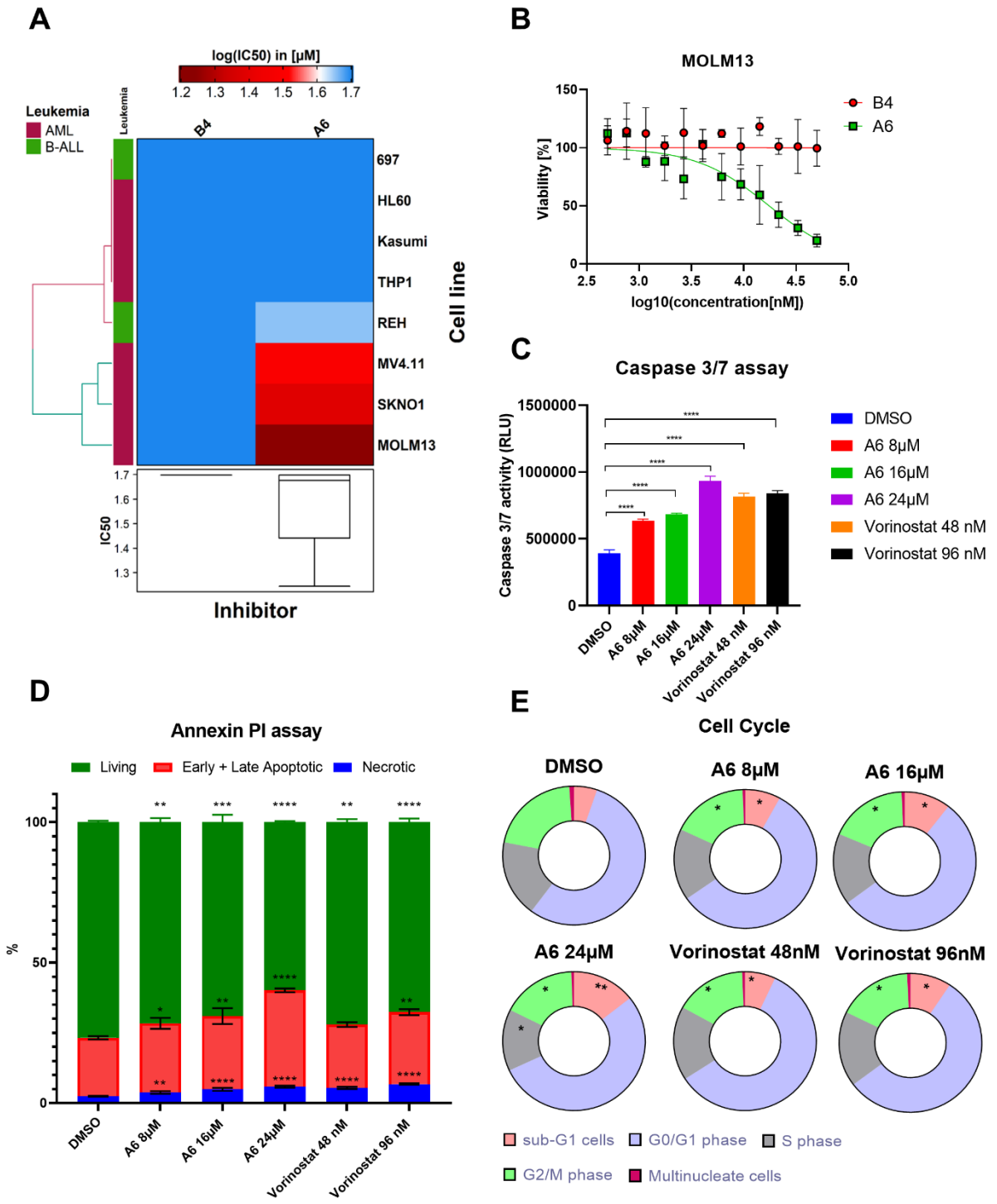

Figure 5: **A.** Comparative cellular viability (log IC_{50} (nM)) of different sub-groups of leukemic cell lines (697, HL-60, KASUMI-1, MV4-11, REH, THP-1, SKNO-1, MOLM-13) after exposure of **A6** or **B4** for 72 h (n=3). The IC_{50} data are plotted as a clustered heat map, followed by unsupervised hierarchical clustering. The vertical axis of the dendogram exemplifies the dissimilarity between clusters, whereas the color of the cell is related to its position along a log IC_{50} (nM) gradient. The boxplot shows the median IC_{50} (log IC_{50} (nM)) of the respective degrader across all tested leukemic cell lines. **B.** IC_{50} values of **A6** and **B4** in leukemia cell lines used in clustered heat map were calculated using non-linear regression (log(antagonist) vs normalized response – variable slope). Representative example of MOLM13 regression curves shown here. **C.** MOLM-13 cells were treated with indicated

concentrations of **A6**, vorinostat or vehicle (DMSO) for 48 h. Treated cells were incubated with caspase-Glo 3/7 substrate and the enzymatic activity of caspase 3/7 was then examined by using a microplate reader (n=3). **D.** MOLM-13 treated (48 h) cells with indicated concentrations of **A6**, vorinostat or vehicle (DMSO) were stained with annexin V and propidium iodide (PI), and the apoptosis induced by these treatments was then assessed by flow cytometry analysis (n=3). **E.** MOLM-13 treated (48 h) cells with indicated concentrations of **A6**, vorinostat or vehicle (DMSO) were stained with PI. The effect of these treatments on the cell cycle were then assessed by flow cytometry analysis (n=3). Significance analyses of normally distributed data with variance similar between groups, used paired, two-tailed Student's t-test (*P< 0.05, **P< 0.01, ***P< 0.001, ****P< 0.0001).

Conclusion

Using a combination of solution- and solid-phase protocols we synthesized a series of HDAC6 degraders based on non-selective (**A1-7**) and HDAC6-selective (**B1-4**) ligands. Our protocols enabled the fast and efficient synthesis of the desired PROTACs in total yields of up to 71%. In both series, western blotting experiments revealed that the PROTACs containing an 8-aminooctanoic acid-based spacer (**A6** and **B4**) demonstrated the most potent degradation of HDAC6. Although **A6** exhibited rather unselective HDAC6 inhibition, both **A6** as well as the selective HDAC6i **B4** displayed selective HDAC6 degradation. Of note, both degraders did not reduce the protein levels of the control HDAC isoforms HDAC1 (class I) and 4 (class IIa). In addition, automated capillary western blotting was performed to quantify the degradation efficiency of the best HDAC6 degraders. Both **A6** and **B4** demonstrated DC_{50} values in the low nanomolar range (**A6**: 3.4 nM and **B4**: 19.3 nM) and comparable D_{max} values over 80%. Furthermore, we showed that pretreatment of the HL-60 cells by either a HDACi, a CRBN ligand or the proteasome inhibitor MG132 rescued HDAC6 from degradation, suggesting that the degradation of HDAC6 occurs via the formation of a ternary complex and through the ubiquitin-proteasome system. Subsequently, in order to analyze the degradation kinetics of **A6** and **B4**, we performed a CRISPR-mediated HiBiT-tagging of HDAC6 in K562 cells and utilized the HiBiT+LgBiT complementation technology to monitor the reduction of HDAC6 levels over 24 h. Both PROTACs demonstrated similar degradation profiles and the maximum degradation was observed between 5.5 and 7.5 h. Moreover, quantitative MS data did not reveal any significant changes in the overall cellular proteome profile after 6 h treatment of K562 cells with PROTACs **A6** or **B4** at 1 µM. Next, HDAC6 degradation of **A6** and intracellular localization of a fluorescein-labelled PROTAC (**A7**) was determined by fluorescence microscopy, which showed subcellular localization of the PROTAC **A7** in the cytoplasm/nuclear-cytoplasmic interphase. In contrast to An *et al.*,[32] we noticed a shift in the intracellular localization of HDAC6 from cytoplasm/nuclear-cytoplasmic interphase into the nucleus upon **A6** (Figure 4) or **A7** (Figure S9, Supporting Information) exposure. HDAC6 is primarily located in the cytoplasm but a fraction of HDAC6 can enter in the nucleus in response to certain stimuli, where it can act as a transcription

factor.[50] This is likely due to increase shuttling of HDAC6 into nucleus in addition to its degradation, upon HDAC6-PROTAC exposure. In fact, high nuclear HDAC6 protein levels are associated with anti-cancer activity.[50] Notably, PROTAC **A6** exhibited encouraging antiproliferative activity in three AML cell lines and **A6** induced apoptosis of MOLM13 cells in a caspase 3/7 dependent fashion through arresting the cells in sub-G1 phase.

Taken together, considering the powerful ability to degrade HDAC6, promising anti-leukemic activity, and the synthetic accessibility by a rapid and straightforward solid-phase protocol, **A6** can be considered as a promising starting point to develop new therapeutic modalities for HDAC6-driven diseases, while the selective HDAC6 inhibitor and degrader **B4** is a new effective pharmacological tool to study HDAC6 biology.

Experimental Section

Chemistry

General remarks. For all solid-phase reactions a 2-chlorotrityl chloride resin (200-400 mesh, 1.1-1.8 mmol/g) supplied by Iris Biotech was used. The manual solid-phase synthesis was carried out in a PP-reactor equipped with a PE frit (sizes: 2/10/20 mL, pore size 25 µm, MultiSynTech GmbH). Syntheses were carried out after the modification of the resin and determination of the loading capacity of the preloaded resin followed the standard Fmoc-solid-phase method. After resin swelling for 30 min in DMF the standard procedure was performed by repeating the Fmoc-deprotection and amide coupling steps. Completion of each coupling step was monitored via the TNBS-test using a TNBS test kit supplied by TCI. After the last coupling cycle, the PROTACs were cleaved from the resin using the standard cleavage cocktail (5% TFA in CH_2Cl_2 (*v*/*v*), treatment for 1 h at r.t.) and the compounds were purified by preparative RP-HPLC. Fractions containing the desired final compounds were collected and lyophilized yielding the HDAC PROTACs **A1-A6** and **B1-4** with >95% purity in all cases. The FITC-labeled PROTAC **A7**, which was used for fluorescence microscopy studies, was obtained as mixture of isomers in a purity of 88%. The Fmoc-protected building blocks (Fmoc-Ahp-COOH, Fmoc-*N*H-Ph-COOH) and PROTAC **A2** were synthesized as previously published.[34]

Fmoc-deprotection: Piperidine (20% in DMF) was added to the resin and the syringe was shaken for 5 min. The step was repeated once, followed by washing steps with DMF (5 x 2 mL), CH_2Cl_2 (5 x 2 mL) and DMF (5 x 2 mL). After the washing step the needle was changed to prevent reactions with remaining piperidine.

TNBS-test: A small amount of resin-beads was placed in a 0.5 mL micro centrifuge tube. One drop of picrylsulfonic acid (~ 1% in DMF) and two drops of DIPEA (10% in DMF) were added to the resin beads and the resin beads were reacted for 5 min at room temperature.

Test cleavage/cleavage from the resin: For a test cleavage about 2 mg of the dried resin was weighed into a tube and treated with the standard cleavage solution (5% TFA in CH_2Cl_2) for 1 h. After the reaction period was finished, the filtrate was collected and the solvent was removed *in vacuo* giving the crude products, which were solvated in milliQ H_2O/MeCN for analytical purposes via HPLC. A cleavage on a larger scale was carried out in the same way. For each 40 mg of resin 1.0 mL of cleavage cocktail was used.

Determination of the loading of the preloaded resin: A small part of the respective preloaded resin (~5 mg) was weighed and treated with 500 µL of the deprotection solution (20% piperidine in DMF) for 5 min. The filtrate was collected, and the procedure was repeated once. The absorbance of the combined filtrates was measured at 300 nm and the concentration was determined photometrically ($\varepsilon_{300\ nm}$(dibenzofulvene) = 7800 $M^{-1}cm^{-1}$).

Nuclear Magnetic Resonance Spectroscopy (NMR): Proton (^{1}H), fluorine (^{19}F) and carbon (^{13}C) NMR spectra were recorded either on a *Bruker* AVANCE III HD 400 MHz or *Varian/Agilent* MERCURYplus 400 at a frequency of 400 MHz (^{1}H), 377 MHz (^{19}F) and 100 MHz (^{13}C) or a *Varian/Agilent* MERCURYplus 300 at a frequency of 300 MHz (^{1}H), 282 MHz (^{19}F) and 75 MHz (^{13}C) or a Bruker Fourier 300 at a frequency of 300 MHz (^{1}H) and 75 MHz (^{13}C). The residual solvent signal ($CDCl_3$: ^{1}H-NMR: 7.26 ppm, ^{13}C-NMR: 77.16 ppm, DMSO-d_6: ^{1}H-NMR: 2.50 ppm, ^{13}C-NMR: 39.52 ppm) was used for calibration referred to tetramethylsilane. As solvents deuterated chloroform ($CDCl_3$) and deuterated dimethyl sulfoxide (DMSO-d_6) were used. The chemical shifts are given in parts per million (ppm). The multiplicity of each signal is reported as singlet (s), doublet (d), triplet (t), quartet (q), multiplet (m) or combinations thereof. Multiplicities are reported as they were measured, and they might disagree with the expected multiplicity of a signal.

Mass Spectrometry: High resolution electrospray ionisation mass spectra (HR-ESI-MS) were acquired either with a *Bruker Daltonik GmbH* microTOF coupled to a *LC Packings* Ultimate HPLC system and controlled by micrOTOFControl3.4 and HyStar 3.2-LC/MS or with a *Bruker Daltonik GmbH* ESI-qTOF Impact II coupled to a *Dionex* UltiMate™ 3000 UHPLC system and controlled by micrOTOFControl 4.0 and HyStar 3.2-LC/MS.

High Performance Liquid Chromatography (HPLC): For analytical purposes a *Thermo Fisher Scientific* UltiMate™ 3000 UHPLC system with a Nucleodur 5 u C18 100 Å (250 x 4.6 mm, Macherey Nagel) column was used. A flow rate of 1 mL/min and a temperature of 25° C were set. For preparative purposes either a *Varian* ProStar or *Knauer* Azura system with either a Jupiter 5 u C18 100 Å-column (250 x 10 mm, Phenomenex) with 4 mL/min or a Nucleodur 5 u C18 HTec (150 x 32 mm, Macherey Nagel) column with 15 mL/min were used. Detection was implemented by UV absorption measurement at a wavelength of λ = 220 nm and λ = 254 nm. Bidest. H_2O (A) and MeCN (B) were used as eluents with an addition of 0.1% TFA to eluent A. For analytical as well as preparative purposes after column

equilibration for 5 min a linear gradient from 5% A to 95% B in 15 min followed by an isocratic regime of 95% B for 5 min was used.

UV-VIS and Infrared Spectroscopy (IR): Loading determinations were performed on a *Shimadzu* UV-160A spectrometer at room temperature. All measurements were performed in a 3500 µL quartz cuvette (100-QS, Hellma Analytics) with a path length of 10 mm. Infrared spectroscopy measurements were performed on a PerkinElmer SpectrumTwo FT-IR spectrometer at room temperature.

General Procedure A. To a cooled (0 °C) solution of the appropriate amine (1.00 equiv.) in 10% aq. Na_2CO_3/1,4-dioxane (3:2, 20mL/mmol) was added Fmoc-Cl (1.5 equiv.) in five portions. The mixture was then allowed to warm to room temperature and stirred for 18 h. Upon completion of the reaction, the solution was diluted with dest. H_2O (30 mL) and washed with Et_2O (3 x 40 mL). Subsequently the aqueous phase was acidified to pH 1 with 6 M HCl. Filtration of the resulting precipitate, followed by washing with dest. H_2O (100 mL) and drying *in vacuo* afforded the desired Fmoc-protected linker.

General Procedure B. The amounts of reagents and solvents used in the following synthesis protocol correspond to a 3.00 – 4.00 mmol scale. After swelling of the 2-chlorotrityl chloride resin (2.00 g, 3.20 mmol, 1.00 equiv., loading 1.60 mmol/g) for 30 min in DMF, a solution of *N*-hydroxyphthalimide (1.88 g, 11.5 mmol, 3.50 equiv.) and Et_3N (1.60 mL, 11.5 mmol, 3.50 equiv.) in DMF (1.5 mL/g resin) was added to the resin and reacted for 48 h. Afterwards, the resin was washed with DMF (10 x 5 mL) and CH_2Cl_2 (10 x 5 mL). Capping of the modified resin was performed by treatment with a capping solution (CH_2Cl_2/MeOH/DIPEA, 80:15:5) two times for 15 min. Subsequently, the resin was washed with CH_2Cl_2 (10 x 5 mL) and dried *in vacuo* to afford the modified resin **5**.

General Procedure C. The amounts of reagents and solvents used in the following synthesis protocol correspond to a 0.09 – 0.20 mmol scale. After the HDACi-preloaded resin (1.00 equiv.) was left to swell for 30 min in DMF, Fmoc deprotection was performed by treatment with 20% piperidine in DMF (1.5 mL, 2 x 5 min). Afterwards, the resin was washed with DMF (5 x 3 mL), CH_2Cl_2 (5 x 3 mL) and DMF (5 x 3 mL). For the subsequent amide coupling reaction, a solution of the appropriate spacer Fmoc-R^2-COOH (3.00 equiv.), HATU (3.00 equiv.), and DIPEA (4.00 equiv.) in DMF (1 mL/mmol acid) was agitated for 5 min and then added to the resin. After 4 h at room temperature the resin was washed with DMF (5 x 3 mL) and CH_2Cl_2 (5 x 3 mL) and completion of the reaction was monitored via the TNBS-test. Again, washing with DMF (5 x 3 mL) and the repetition of the Fmoc-deprotection step give the free amine which was reacted further in the last coupling cycle with the respective CRBN building block (1.50

– 2.20 equiv.), HATU (2.00 – 2.20 equiv.) and DIPEA (3.00 – 4.00 equiv.) in DMF (500 µL) for 4 h at room temperature. After washing with DMF (5 x 3 mL) and CH_2Cl_2 (5 x 3 mL) and negative TNBS-test, the resin was dried *in vacuo* followed by the cleavage of the crude products from the resin and purification *via* preparative HPLC.

2-Methyl-6-nitro-1*H*-benzo[*d*]imidazole (1). 4-Nitrobenzene-1,2-diamine (3.06 g, 20 mmol, 1.00 equiv.) was dissolved in MeOH (8 mL). Triethyl orthoacetate (4.40 mL, 24 mmol, 1.20 equiv.) and sulfamic acid (19.4 mg, 0.20 mmol, 1 mol%) were added to the solution and the mixture was stirred for 4 h at room temperature. Afterwards, the solvent was removed under reduced pressure and the product was resuspended in EtOAc and filtered. Subsequent purification by flash column chromatography using CH_2Cl_2/MeOH (gradient 0-10 %) gave the desired product **1** as beige solid (2.78 g, 15.7 mmol, 79%). **^{1}H-NMR** (400 MHz, DMSO-d_6, δ): 12.88 (s, 1H), 8.35 (dd, *J* = 2.3, 0.5 Hz, 1H), 8.05 (dd, *J* = 8.8, 2.3 Hz, 1H), 7.62 (dd, *J* = 8.8, 0.6 Hz, 1H), 2.56 (s, 3H) ppm. **HRMS-ESI (*m/z*)**: $[M + H]^+$ calcd for $C_8H_7N_3O_2$: 178.0611, found: 178.0618. Analytical data are in agreement with literature.[51]

Methyl 4-(bromomethyl)-3-fluorobenzoate (2). Compound **16** (3.36 g, 20.0 mmol, 1.00 equiv.) was dissolved in $CHCl_3$ (80 mL) under vigorous stirring. NBS (5.34 g, 30.0 mmol, 1.50 equiv.) and AIBN (0.66 g, 4.02 mmol, 0.20 equiv.) were added and the orange reaction mixture was stirred for 16 h at 80 °C. The solvent was removed under reduced pressure and the yellow/orange residue was purified by flash column chromatography (cyclohexane/EtOAc, 98:2), yielding the desired product **2** as light yellowish solid (3.34 g, 13.5 mmol, 68%). **^{1}H-NMR** (400 MHz, $CDCl_3$, δ): 7.81 (dd, *J* = 8.0, 1.6 Hz, 1H), 7.72 (dd, *J* = 10.2, 1.6 Hz, 1H), 7.47 (t, *J* = 7.7 Hz, 1H), 4.52 (d, *J* = 1.1 Hz, 2H), 3.93 (s, 3H) ppm. **^{19}F-NMR** (377 MHz, $CDCl_3$, δ): -116.05 (m) ppm.**^{13}C-NMR** (101 MHz, $CDCl_3$, δ): 165.6 (d, $^4J_{C\text{-}F}$ = 2.8 Hz), 160.4 (d, $^1J_{C\text{-}F}$ = 251.1 Hz), 132.6 (d, $^3J_{C\text{-}F}$ = 7.7 Hz), 131.4 (d, $^3J_{C\text{-}F}$ = 3.1 Hz), 130.2 (d, $^2J_{C\text{-}F}$ = 14.7 Hz), 125.8 (d, $^4J_{C\text{-}F}$ = 3.7 Hz), 117.1 (d, $^2J_{C\text{-}F}$ = 23.3 Hz), 52.6, 24.7 (d, $^3J_{C\text{-}F}$ = 4.3 Hz) ppm. Analytical data are in agreement with literature.[52]

Methyl 3-fluoro-4-((2-methyl-5-nitro-1*H*-benzo[*d*]imidazol-1-yl)methyl)benzoate (3). **1** (1.42 g, 8.02 mmol, 1.00 equiv.) and **2** (1.98 g, 8.01 mmol, 1.00 equiv.) were dissolved in THF (40 mL). Cs_2CO_3 (5.21 g, 16.0 mmol, 2.00 equiv.) was added to the resulting yellow solution. The reaction was stirred for 2 h at 80 °C. Afterwards, the reaction was cooled to room temperature, diluted with dist. H_2O (28 mL), and extracted with EtOAc (3 x 60 mL). The combined organic layers were washed with brine (1 x 70 mL) and dried over anhydrous $MgSO_4$. After filtration and removal of the solvent *in vacuo*, the crude product

was purified by flash column chromatography (cyclohexane/EtOAc, 30:70), yielding the main isomer **3** as beige solid (1.21 g, 3.52 mmol, 44%). **^{1}H-NMR** (400 MHz, $CDCl_3$, δ): 8.62 (d, *J* = 2.1 Hz, 1H), 8.16 (dd, *J* = 8.9, 2.1 Hz, 1H), 7.80 (dd, *J* = 10.5, 1.6 Hz, 1H), 7.74 (dd, *J* = 8.0, 1.6 Hz, 1H), 7.29 (d, *J* = 8.9 Hz, 1H), 6.83 (t, *J* = 7.6 Hz, 1H), 5.47 (s, 2H), 3.91 (s, 3H), 2.67 (s, 3H) ppm. **^{19}F-NMR** (377 MHz, $CDCl_3$, δ): -116.42 ppm. **^{13}C-NMR** (101 MHz, $CDCl_3$, δ): 165.3 (d, $^{4}J_{C\text{-}F}$ = 2.5 Hz), 160.0 (d, $^{1}J_{C\text{-}F}$ = 248.5 Hz), 155.7, 144.1, 141.9, 139.3, 132.9 (d, $^{3}J_{C\text{-}F}$ = 7.7 Hz), 128.0 (d, $^{3}J_{C\text{-}F}$ = 3.4 Hz), 126.9 (d, $^{2}J_{C\text{-}F}$ = 14.6 Hz), 126.2 (d, $^{4}J_{C\text{-}F}$ = 3.6 Hz), 118.8, 117.3 (d, $^{2}J_{C\text{-}F}$ = 22.9 Hz), 116.0, 109.3, 52.8, 42.0 (d, $^{3}J_{C\text{-}F}$ = 4.7 Hz), 14.3 ppm. **HRMS-ESI (*m/z*)**: $[M + H]^+$ calcd for $C_{17}H_{14}FN_3O_4$: 344.1041, found: 344.1057.

4-((5-((((9H-Fluoren-9-yl)methoxy)carbonyl)amino)-2-methyl-1*H*-benzo[*d*]imidazol-1-yl)methyl)-3-fluorobenzoic acid (4). 10% Pd/C (124 mg) was added to a solution of **3** (1.24 g, 3.61 mmol, 1.00 equiv.) in MeOH/CH_2Cl_2 (5:1, 120 mL) and the reaction was vigorously stirred under H_2-atmosphere. Full conversion was detected via HPLC after 4 h. The reaction solution was filtered through Celite® and the solvent was removed *in vacuo*. The light orange oily residue was dissolved in THF/MeOH (5:1, 90 mL) and $NaOH_{aq.}$ (50 mg/mL, 11.5 mL, 14.4 mmol, 4.00 equiv.) was added to the solution. Full conversion was monitored after 2 h via HPLC. The reaction solution was neutralized with 1 M $HCl_{aq.}$(14.4 mL, 14.4 mmol, 4.00 equiv.) and the solvent was removed *in vacuo*. The residue was dissolved in 5% $Na_2CO_{3\ aq.}$/1,4-dioxane (3:2, 60 mL) and Fmoc-Cl (1.40 g, 5.41 mmol, 1.50 equiv.) was added carefully in five portions at 0 °C. After stirring for 18 h the reaction solution was acidified with 6 M HCl to pH 4 and the precipitate was filtered, washed with water and dried *in vacuo* yielding the desired product **4** as beige solid (1.54 g, 2.95 mmol, 82%). **Mp**: 193 °C (decomp.). **^{1}H-NMR** (300 MHz, DMSO-d_6, δ): 10.01 (s, 1H), 7.99 (s, 1H), 7.92 (s, 1H), 7.90 (s, 1H), 7.77 (s, 1H), 7.76 – 7.73 (m, 2H), 7.73 – 7.70 (m, 1H), 7.63 (d, *J* = 9.0 Hz, 1H), 7.39 (dtd, *J* = 24.2, 7.4, 0.9 Hz, 7H), 5.77 (s, 2H), 4.52 (d, *J* = 6.6 Hz, 2H), 4.32 (t, *J* = 6.6 Hz, 1H), 2.77 (s, 3H) ppm. **^{19}F-NMR** (377 MHz, DMSO-d_6, δ): -115.78 (t, *J* = 8.9 Hz) ppm.**^{13}C-NMR** (101 MHz, DMSO-d_6, δ): 166.0 (d, $^{4}J_{C\text{-}F}$ = 1.8 Hz), 163.2, 159.5 (d, $^{1}J_{C\text{-}F}$ = 246.6 Hz), 153.7, 152.5, 143.8, 142.4, 140.8, 133.6 (d, $^{4}J_{C\text{-}F}$ = 1.9 Hz), 131.3, 128.7 (d, $^{3}J_{C\text{-}F}$ = 4.2 Hz), 128.5 (d, $^{2}J_{C\text{-}F}$ = 14.8 Hz), 127.7, 127.1, 125.7 (d, $^{3}J_{C\text{-}F}$ = 3.3 Hz), 125.2, 120.2, 116.0 (d, $^{2}J_{C\text{-}F}$ = 22.3 Hz), 109.6, 65.5, 46.7, 41.0 (d, $^{3}J_{C\text{-}F}$ = 3.3 Hz), 13.5 ppm. **HRMS-ESI (*m/z*)**: $[M + H]^+$ calcd for $C_{31}H_{24}FN_3O_4$: 522.1824, found: 522.1825. **IR**: $\tilde{\nu}$= 3388 (w), 2872 (br), 2566 (br), 2346 (br), 1807 (br), 1720 (s), 1702 (m), 1621 (w), 1582 (w), 1536 (m), 1506 (m), 1427 (w), 1415 (w), 1329 (w), 1277 (m), 1220 (vs), 1182 (m), 1115 (w), 1083 (m), 1049 (m), 1006 (w), 961 (w), 933 (m), 855 (w), 803 (m), 760 (m), 737 (s), 675 (w), 632 (w), 614 (m), 565 (m), 538 (m), 505 (w), 472 (w) cm^{-1}.

Non-selective HDACi precursor (6). After swelling of the modified resin **5** (500 mg, estimated loading 1.50 mmol/g, 0.75 mmol, 1.00 equiv.) for 30 min in DMF, the resin was washed with MeOH (3 x 5 mL). The phthaloyl protecting group was removed by treatment with 5% hydrazine monohydrate in MeOH for 15 min (2 x 3 mL). Afterwards, the resin was washed with DMF (3 x 5 mL), MeOH (3 x 5 mL), CH_2Cl_2 (3 x 5 mL) and DMF (3 x 5 mL). For the subsequent amide coupling reaction, a solution of Fmoc-aminoheptanoic acid (551 mg, 1.50 mmol, 2.00 equiv.), HATU (570 mg, 1.50 mmol, 2.00 equiv.), HOBt·H_2O (230 mg, 1.50 mmol, 2.00 equiv.) and DIPEA (383 µL, 2.25 mmol, 3.00 equiv.) in DMF (2 mL) was agitated for 5 min and then added to the resin. The amide coupling was performed for 20 h at room temperature. Afterwards, the resin was washed with DMF (3 x 5 mL) and CH_2Cl_2 (3 x 5 mL). Completion of the reaction was monitored via TNBS-test. Upon completion of the reaction and washing, the resin **17** was dried *in vacuo* and a loading between 0.77 mmol/g and 0.97 mmol/g was photometrically determined for different batches. The dried resin was stored at 4 °C.

After swelling of the resin **17** (676 mg, 0.97 mmol/g, 0.65 mmol, 1,00 eq) in DMF for 30 min, Fmoc-deprotection was performed by treatment with 20% piperidine in DMF. Afterwards, the resin was washed with DMF (3x5 mL), CH_2Cl_2 (3x5 mL) and DMF (3x5 mL). For the subsequent amide coupling reaction, a solution of Fmoc-aminobenzoic acid (701 mg, 1.95 mmol, 3.00 equiv.), HATU (741 mg, 1.95 mmol, 3.00 equiv.), and DIPEA (454 µL, 2.60 mmol, 4.00 equiv.) in DMF (1.5 mL) was agitated for 5 min and then added to the resin. After a reaction time of 20 h at room temperature, the resin was washed with DMF (3x5 mL) and CH_2Cl_2 (3x5 mL). Completion of the reaction was monitored via the TNBS-test. The resin was dried *in vacuo* and stored at 4 °C.

Selective HDAC6i precursor (7). After swelling of the modified resin **5** (133 mg, estimated loading 1.50 mmol/g, 0.20 mmol, 1.00 equiv.) for 30 min in DMF, the resin was washed with MeOH (3 x 3 mL). The phthaloyl protecting group was removed by treatment with 5% hydrazine monohydrate in MeOH for 15 min (2 x 1.5 mL). Afterwards, the resin was washed with DMF (3 x 3 mL), MeOH (3 x 3 mL), CH_2Cl_2 (3 x 3 mL) and DMF (3 x 3 mL). For the subsequent amide coupling reaction, a solution of **4** (208 mg, 0.40 mmol, 2.00 equiv.), HATU (152 mg, 0.40 mmol, 2.00 equiv.), HOBt·H_2O (61.0 mg, 0.40 mmol, 2.00 equiv.) and DIPEA (102 µL, 0.60 mmol, 3.00 equiv.) in DMF (900 µL) was agitated for 5 min and then added to the resin. The amide coupling was performed for 20 h at room temperature. Afterwards, the resin was washed with DMF (3 x 3 mL) and CH_2Cl_2 (3 x 3 mL). Completion of the reaction was

monitored via the TNBS-test. Upon completion of the reaction and washing, the resin was dried *in vacuo* and a loading of 0.60 – 0.62 mmol/g was photometrically determined for different batches of the preloaded resin. The dried resin was stored at 4 °C.

8-((((9*H*-Fluoren-9-yl)methoxy)carbonyl)amino)octanoic acid (8a). Synthesized from 8-aminooctanoic acid (500 mg, 3.14 mmol, 1.00 equiv.) and 9-fluorenylmethoxy-carbonyl chloride (1.22 g, 4.71 mmol, 1.50 equiv.) according to general procedure A afforded the desired product **8** as white solid (675 mg, 1.77 mmol, 56%). **^{1}H-NMR** (400 MHz, $CDCl_3$, δ): 7.79 (dt, *J* = 7.6, 1.0 Hz, 2H), 7.62 (dd, *J* = 7.6, 1.1 Hz, 2H), 7.46 – 7.38 (m, 2H), 7.34 (td, *J* = 7.4, 1.2 Hz, 2H), 4.78 (s, 1H), 4.43 (d, *J* = 6.9 Hz, 2H), 4.24 (t, *J* = 7.0 Hz, 1H), 3.27 – 3.04 (m, 2H), 2.38 (t, *J* = 7.4 Hz, 2H), 1.66 (p, *J* = 7.3 Hz, 2H), 1.52 (t, *J* = 7.0 Hz, 2H), 1.43 – 1.27 (m, 6H) ppm. **HRMS-ESI (*m/z*)**: [*M* + Na]$^+$ calcd for $C_{23}H_{27}NO_4$: 404.1832, found: 404.1834. The analytical data are are in agreement with the literature.[53]

***tert*-Butyl (2,6-dioxopiperidin-3-yl)carbamate (9).** To a solution of Boc-l-Gln-OH (10.0 g, 40.6. mmol, 1.00 equiv.) in dry THF (100 mL) was added CDI (7.00 g, 43.7 mmol, 1.08 equiv.) and DMAP (21.0 mg, 0.17 mmol, 0.42 mol%). The reaction was heated to reflux for 24 h under argon atmosphere. The reaction mixture was concentrated to about half of the original volume *in vacuo* resulting in precipitation of the desired product, which was filtrated and washed with cold THF. Repeating this procedure once gave the desired product **9** as white solid (4.53 g, 19.9 mmol, 49%). **^{1}H-NMR** (300 MHz, DMSO-d_6, δ): 10.72 (s, 1H), 7.11 (d, *J* = 8.7 Hz, 1H), 4.22 (q, *J* = 8.8 Hz, 1H), 2.81 – 2.60 (m, 1H), 2.44 (q, *J* = 4.0 Hz, 1H)*, 2.02 – 1.83 (m, 2H), 1.39 (s, 9H) ppm, *partially overlapping with DMSO signal. **HRMS-ESI (*m/z*)**: [*M* + Na]$^+$ calcd for $C_{10}H_{16}N_2O_4$: 251.1002, found: 251.1009. Analytical data are in agreement with the literature.[53]

2-(2,6-Dioxopiperidin-3-yl)-4-hydroxyisoindoline-1,3-dione (10). 4-Hydroxyisobenzofuran-1,3-dione (492 mg, 3.00 mmol, 1.50 equiv.) was suspended in acetic acid (20 mL). **9** (457 mg, 2.00 mmol, 1.00 eq) and NaOAc (131 mg, 1.60 mmol, 0.80 eq) were added and the mixture was heated under reflux for 6 h. After expiration of this time, the reaction solution was cooled to room temperature. The mixture was diluted with H_2O (100 mL) and extracted with CH_2Cl_2 (10 x 50 mL). The combined organic phases were dried over anhydrous $MgSO_4$, filtered, and the solvent was removed *in vacuo*. The crude product was purified by flash column chromatography (CH_2Cl_2/MeOH, 0 → 10%) yielding the desired product **10** as beige solid (319 mg, 1.16 mmol, 39%). **^{1}H-NMR** (400 MHz, DMSO-d_6, δ): δ 11.19 (s, 1H, broad signal), 11.08 (s, 1H), 7.65 (dd, J = 8.4, 7.2 Hz, 1H), 7.32 (d, J = 7.1 Hz, 1H), 7.28 – 7.19 (m, 1H), 5.07 (dd, J =

12.9, 5.4 Hz, 1H), 2.95 – 2.82 (m, 1H), 2.64 – 2.45* (m, 2H), 2.07 – 1.98 (m, 1H) ppm, *partially overlapping with DMSO-signal. **HRMS-ESI (m/z)**: $[M + Na]^+$ calcd for $C_{13}H_{10}N_2O_5$: 297.0482, found: 297.0494. Analytical data are in agreement with literature.[53]

Benzyl 2-((2-(2,6-dioxopiperidin-3-yl)-1,3-dioxoisoindolin-4-yl)oxy)acetate (11). DIAD (950 µL, 4.84 mmol, 1.10 equiv.) was added dropwise under argon atmosphere to a cooled (0 °C) solution of **10** (1.20 g, 4.40 mmol, 1.00 equiv.), PPh_3 (1.73 g, 6.60 mmol, 1.50 equiv.) and benzyl glycolate (687 µL, 4.84 mmol, 1.10 equiv.) in dry THF (50 mL). The reaction was allowed to warm to room temperature and stirred for 20 h. Afterwards, the reaction was quenched with dest. H_2O (50 mL) and diluted with EtOAc (50 mL). The aqueous phase was washed with EtOAc (3 x 50 mL) and the combined organic phases were dried over anhydrous $MgSO_4$, filtered, and concentrated *in vacuo*. The crude product was purified three times in total by flash column chromatography (cyclohexane/EtOAc) using a linear gradient from 5-95% EtOAc in 30 min yielding **11** as a white foam (985 mg, 2.33 mmol, 53 %).**^{1}H-NMR** (300 MHz, $CDCl_3$, δ): 8.12 (s, 1H), 7.62 (dd, *J* = 8.4, 7.3 Hz, 1H), 7.55 – 7.48 (m, 1H), 7.34 (d, *J* = 1.1 Hz, 5H), 7.08 (dd, *J* = 8.5, 0.8 Hz, 1H), 5.23 (s, 2H), 4.98 (d, *J* = 5.5 Hz, 1H), 4.94 (s, 2H), 3.03 – 2.61 (m, 3H), 2.24 – 2.07 (m, 1H) ppm.**^{13}C-NMR** (75 MHz, DMSO-d_6, δ): 171.0, 168.0, 167.9, 166.9, 165.5, 155.4, 136.5, 135.0, 134.1, 128.8, 128.8, 128.7, 120.3, 117.9, 117.3, 67.5, 66.5, 49.3, 31.5, 22.7 ppm. **HRMS-ESI (*m/z*)**: $[M + Na]^+$ calcd for $C_{22}H_{18}N_2O_7$: 445.1006, found: 445.1004. Analytical data are in agreement with literature.[53]

2-((2-(2,6-Dioxopiperidin-3-yl)-1,3-dioxoisoindolin-4-yl)oxy)acetic acid (12). 10% Pd/C (28 mg) was added to a solution of **11** (280 mg, 0.66 mmol, 1.00 equiv.) in 2.5:1 EtOAc/CH_2Cl_2 (30 mL) and the reaction was vigorously stirred under H_2-atmosphere. During the reaction a grey suspension formed and more precipitation occurred. After 4 h the reaction was gently flushed with argon and the mixture was diluted with MeOH (50 mL). The reaction mixture was heated carefully to reflux and filtered through celite®. The celite® was washed with hot MeOH (200 mL) and the combined organic phases were dried *in vacuo* yielding **12** as white solid (210 mg, 0.63 mmol, 95%), which was used for solid-phase synthesis without further purification. **^{1}H-NMR** (400 MHz, DMSO-d_6, δ): 11.10 (s, 1H), 7.79 (dd, *J* = 8.5, 7.3 Hz, 1H), 7.47 (d, *J* = 7.2 Hz, 1H), 7.38 (d, *J* = 8.5 Hz, 1H), 5.10 (dd, *J* = 12.8, 5.4 Hz, 1H), 4.96 (s, 2H), 2.89 (ddd, *J* = 17.3, 14.0, 5.3 Hz, 1H), 2.66 – 2.45 (m, 2H)*, 2.09 – 1.97 (m, 1H) ppm, *partially overlapping with DMSO signal.**^{13}C-NMR** (101 MHz, DMSO-d_6, δ): 172.8, 169.9, 169.5, 166.8, 165.2, 155.2, 136.7,

133.2, 119.9, 116.3, 115.7, 65.1, 48.8, 31.0, 22.0 ppm. **HRMS-ESI (*m/z*)**: [*M* + Na]$^+$ calcd for $C_{15}H_{12}N_2O_7$: 355.0537, found: 355.0545. Analytical data are in agreement with literature.[53]

2-(2,6-Dioxopiperidin-3-yl)-4-fluoroisoindoline-1,3-dione (13). 3-Fluorophthalic anhydride (3.08 g, 18.6 mmol, 1.50 equiv.) was suspended in glacial acetic acid (60 mL). **9** (2.83 g, 12.4 mmol, 1.00 eq) and NaOAc (814 mg, 9.92 mmol, 0.80 eq) were added and the mixture was heated to reflux for 6 h. The solution was cooled to room temperature and poured into H_2O (150 mL). The precipitate was collected by filtration and washed with H_2O (50 mL) and petroleum ether (30 mL). The solid was dried *in vacuo* yielding the desired product **13** (2.47 g, 8.93 mmol, 72%) as grey solid. **^{1}H-NMR** (400 MHz, DMSO-d_6, δ): 11.14 (s, 1H), 7.95 (ddd, *J* = 8.4, 7.3, 4.5 Hz, 1H), 7.79 (d, *J* = 7.3 Hz, 1H), 7.73 (t, *J* = 8.9 Hz, 1H), 5.16 (dd, *J* = 12.8, 5.4 Hz, 1H), 2.89 (ddd, *J* = 17.1, 13.9, 5.4 Hz, 1H), 2.66 – 2.43* (m, 2H), 2.07 (dtd, *J* = 13.0, 5.3, 2.3 Hz, 1H) ppm, *partially overlapping with DMSO-signal. **^{19}F NMR** (377 MHz, DMSO-d_6, δ): -114.65 (dd, *J* = 9.5, 4.5 Hz) ppm. **HRMS-ESI (*m/z*)**: [*M* + Na]$^+$ calcd for $C_{13}H_9FN_2O_4$: 299.0439, found: 299.0456. Analytical data are in agreement with literature.[54]

Benzyl (2-(2,6-dioxopiperidin-3-yl)-1,3-dioxoisoindolin-4-yl)glycinate (14). 13 (300 mg, 1.09 mmol, 1.00 equiv.), H-Gly-OBz (269 mg, 1.63 mmol, 1.50 equiv.) was dissolved in DMF (5 mL) and DIPEA (285 µL, 1.63 mmol, 1.50 equiv.) was added to the solution. The reaction mixture was agitated at 150 °C for 5 min in a microwave assisted reaction (150 W). The solution was cooled to room temperature and the solvent was coevaporated with toluene (3 x 10 mL). Purification by preparative HPLC afforded **14** as yellow powder (113 mg, 0.27 mmol, 25%). **^{1}H-NMR** (400 MHz, $CDCl_3$, δ): 8.12 (s, 1H), 7.49 (dd, *J* = 8.5, 7.2 Hz, 1H), 7.41 – 7.31 (m, 5H), 7.17 (dd, *J* = 7.1, 0.6 Hz, 1H), 6.81 – 6.61 (m, 1H), 6,69 (s, broad signal, 1H) 5.23 (s, 2H), 5.03 – 4.85 (m, 1H), 4.10 (s, 2H), 2.99 – 2.65 (m, 3H), 2.21 – 2.07 (m, 1H) ppm.**^{13}C-NMR** (101 MHz, $CDCl_3$-d_1, δ): 171.2, 169.6, 169.2, 168.3, 167.6, 145.8, 136.3, 135.2, 132.7, 128.8, 128.8, 128.7, 116.8, 112.8, 111.4, 67.6, 49.1, 44.6, 31.5, 22.9 ppm. **HRMS-ESI (*m/z*)**: [*M* + Na]$^+$ calcd for $C_{22}H_{19}N_3O_6$: 444.1166, found: 444.1176. **IR**: $\tilde{\nu}$= 3261 (br), 2871 (br), 1694 (s), 1625 (m), 1503 (m), 1407 (m), 1359 (m), 1320 (w), 1259 (m), 1197 (s), 1114 (s), 952 (w), 835 (w), 814 (w), 747 (m), 719 (m), 600 (w), 467 (w) cm^{-1}.

(2-(2,6-Dioxopiperidin-3-yl)-1,3-dioxoisoindolin-4-yl)glycine (15). 10% Pd/C (24.9 mg) was added to a solution of **14** (249 mg, 0.59 mmol, 1.00 equiv.) in 1:2 MeOH/CH_2Cl_2 (25 mL) and the reaction was vigorously stirred under H_2-atmosphere. After 2 h full conversion was monitored by RP-HPLC. After change of the atmosphere, the reaction was diluted with warm MeOH (50 mL). The suspension was

filtered through celite® and the celite® was washed with warm MeOH until the celite® pad has lost its yellow color. The combined organic phases were dried *in vacuo* and lyophilized yielding **15** as yellow solid (176 mg, 0.53 mmol, 90%). The product was used without further purification. **HPLC**: t_R= 14.28 min. **^{1}H-NMR** (400 MHz, DMSO-d_6, δ): δ 11.10 (s, 1H), 7.58 (dd, *J* = 8.5, 7.1 Hz, 1H), 7.07 (d, *J* = 7.1 Hz, 1H), 6.98 (d, *J* = 8.5 Hz, 1H), 6.86 (t, *J* = 5.7 Hz, 1H), 5.07 (dd, *J* = 12.9, 5.4 Hz, 1H), 4.07 (d, *J* = 5.7 Hz, 2H), 2.89 (ddd, *J* = 17.3, 13.9, 5.4 Hz, 1H), 2.65 – 2.52* (m, 2H), 2.07 – 1.99 (m, 1H) ppm, *partially overlapping with DMSO-signal, N*H* could not be detected due to solvent exchange.**^{13}C-NMR** (101 MHz, DMSO-d_6, δ): 172.8, 171.4, 170.1, 168.8, 167.3, 145.8, 136.1, 132.0, 117.7, 111.0, 109.6, 48.6, 43.9, 31.0, 22.1. **HRMS-ESI (*m/z*)**: [*M* + Na]$^+$ calcd for $C_{15}H_{13}N_3O_6$: 354.0697, found: 354.0704. **IR**: $\tilde{\nu}$= 3377 (w), 3182 (br), 3089 (br), 2906 (br), 1745 (w), 1688 (s), 1621 (m), 150 (w), 1445 (w), 1399 (m), 1295 (w), 1264 (m), 1198 (s), 1179 (m), 1148 (m), 1106 (m), 1017 (w), 945 (w), 921 (w), 814 (m), 741 (s), 679 (w), 601 (s), 471 (s) cm^{-1}.

Methyl 3-fluoro-4-methylbenzoate (16). Thionyl chloride (3.06 mL, 42.2 mmol, 1.30 equiv.) was added dropwise to a cooled (0 °C) solution of 3-fluoro-4-methylbenzoic acid (5.00 g, 32.4 mmol, 1.00 equiv.) in dry MeOH (150 mL). The reaction was allowed to warm to room temperature and stirred for further 4 h at 50 °C. Afterwards, the reaction was cooled to 0 °C and gently quenched with 1 M HCl (70 mL). Brine (20 mL) was added and the yellow colored reaction solution was extracted with EtOAc (3 x 100 mL). The combined organic phases were dried over anhydrous Na_2SO_4 and filtrated. Removal of the solvent *in vacuo* yielded the desired product **16** as yellow/brown solid (5.09 g, 30.2 mmol, 93%). **^{1}H-NMR** (400 MHz, $CDCl_3$, δ): 7.72 (dd, *J* = 7.9, 1.7 Hz, 1H), 7.65 (dd, *J* = 10.2, 1.7 Hz, 1H), 7.25 (t, *J* = 7.7 Hz, 1H), 3.91 (s, 3H), 2.33 (d, *J* = 1.8 Hz, 3H) ppm. **^{19}F-NMR** (377 MHz, $CDCl_3$,δ): -116.75 (m) ppm. **^{13}C-NMR** (101 MHz, $CDCl_3$, δ): 166.3 (d, $^4J_{C-F}$ = 2.5 Hz), 161.1 (d, $^1J_{C-F}$ = 245.5 Hz), 131.5 (d, $^3J_{C-F}$ = 5.0 Hz), 130.7 (d, $^2J_{C-F}$ = 17.3 Hz), 129.8 (d, $^3J_{C-F}$= 7.5 Hz), 125.2 (d, $^4J_{C-F}$ = 3.5 Hz), 116.2 (d, $^2J_{C-F}$ = 24.1 Hz), 52.4, 15.0 (d, $^3J_{C-F}$ = 3.6 Hz) ppm. **HRMS-ESI (*m/z*)**: [*M* + Na]$^+$ calcd for $C_9H_9FO_2$: 191.0479, found: 191.0485.

4-(2-(2-(2-((2-(2,6-Dioxopiperidin-3-yl)-1,3-dioxoisoindolin-4-yl)oxy)acetamido)ethoxy) acetamido)-*N*-(7-(hydroxyamino)-7-oxoheptyl)benzamide (A1). Synthesized according to general procedure C using **6** (147 mg, 0.10 mmol, 1.00 eq), Fmoc-O1Pen-OH (102 mg, 0.30 mmol, 3.00 eq), HATU (114 mg, 0.30 mmol, 3.00 equiv.) and DIPEA (70.0 µL, 0.40 mmol, 4.00 equiv.) in DMF (300 µL). The second coupling cycle was performed using the hydroxythalidomide building block **12** (50.0 mg, 0.15 mmol, 1.50 equiv), HATU (76.0 mg, 0.20 mmol, 2.00 equiv.) and DIPEA (52.0 µL, 0.30 mmol, 3.00 equiv.) in DMF (500 µL). Purification by preparative HPLC afforded **A1** as white powder (39.0 mg, 56.1 µmol, 56 %) in >95% purity. **HPLC**: t_R= 13.56 min. **^{1}H-NMR** (400 MHz, DMSO-d_6, δ): 11.10 (s, 1H), 10.32 (s, 1H), 9.77 (s, 1H), 8.29 (t, *J* = 5.6 Hz, 1H), 8.20 (t, *J* = 5.8 Hz, 1H), 7.78 (dd, *J* = 8.6, 7.6 Hz, 3H), 7.72 – 7.62 (m, 2H), 7.45 (d, *J* = 7.2 Hz, 1H), 7.38 (d, *J* = 8.5 Hz, 1H), 5.08 (dd, *J* = 12.8, 5.4 Hz, 1H), 4.82 (s, 2H), 4.08 (s, 2H), 3.60 (t, *J* = 5.5 Hz, 2H), 3.46 – 3.34 (m, 2H*), 3.22 (q, *J* = 6.7 Hz, 2H), 2.87 (ddd, *J* = 16.9, 13.8, 5.4 Hz, 1H), 2.62 – 2.42 (m, 2H), 2.04 – 1.96 (m, 1H), 1.94 (t, *J* = 7.4 Hz, 2H), 1.53 – 1.44 (m, 4H), 1.33 – 1.22 (m, 4H) ppm, *overlaping with water signal -C-N*H*-OH signal could not be detected due to solvent exchange. **^{13}C-NMR** (101 MHz, DMSO-d_6, δ): 172.8, 169.9, 169.1, 168.4, 167.2, 166.7, 165.5, 165.4, 155.1, 140.7, 136.9, 133.0, 129.6, 127.9, 120.3, 118.7, 116.8, 116.0, 70.0, 69.6, 67.6, 48.8,*, 38.3, 32.3, 31.0, 29.1, 28.4, 26.3, 25.1, 22.0 ppm, * overlapping with DMSO-signal. **HRMS-ESI (*m/z*)**: $[M + H]^+$ calcd for $C_{33}H_{38}N_6O_{11}$: 695.2671, found: 695.2695. **IR**: $\tilde{\nu}$ = 3251 (br), 2932 (br), 1774 (w), 1708 (s), 1667 (m), 1615 (m), 1532 (s), 1397 (m), 1261 (m), 1198 (m), 1110 (m), 1056 (m), 1016 (w), 989 (w), 853 (w), 747 (m), 601 (m), 466 (w) cm^{-1}.

4-(1-((2-(2,6-Dioxopiperidin-3-yl)-1,3-dioxoisoindolin-4-yl)oxy)-2-oxo-6,9,12-trioxa-3-azapentadecan-15-amido)-*N*-(7-(hydroxyamino)-7-oxoheptyl)benzamide (A3) Synthesized according to general procedure C using **6** (168 mg, 0.15 mmol, 1.00 eq), Fmoc-NH-PEG(3)-OH (200 mg, 0.45 mmol, 3.00 eq), HATU (171 mg, 0.45 mmol, 3.00 equiv.) and DIPEA (105 µL, 0.60 mmol, 4.00 equiv.) in DMF (500 µL). The second coupling cycle was performed using the hydroxythalidomide building block **12** (99.7 mg, 0.30 mmol, 2.00 equiv), HATU (125 mg, 0.33 mmol, 2.20 equiv.) and DIPEA (92.0 µL, 0.53 mmol, 3.50 equiv.) in DMF (500 µL). Purification by preparative HPLC afforded **A3** as white powder (77.4 mg, 97.0 µmol, 65 %) in >95% purity. **HPLC**: t_R= 13.80 min. **^{1}H-NMR** (400 MHz, DMSO-d_6, δ): 11.11 (s, 1H), 10.32 (s, 1H), 10.11 (s, 1H), 8.28 (t, *J* = 5.6 Hz, 1H), 7.99 (t, *J* = 5.7 Hz, 1H), 7.89 – 7.72 (m, 3H), 7.68 – 7.58 (m, 2H), 7.49 (d, *J* = 7.2 Hz, 1H), 7.39 (d, *J* = 8.5 Hz, 1H), 5.11 (dd, *J* = 12.9, 5.4 Hz, 1H), 4.78 (s, 2H), 3.69 (t, *J* = 6.2 Hz, 2H), 3.56 – 3.47 (m, 8H), 3.44 (t, *J* = 5.7 Hz, 2H), 3.30 (q, *J* = 5.7 Hz, 2H), 3.21 (q, *J* = 6.7 Hz, 2H), 2.89 (ddd, *J* = 17.3, 14.0, 5.4 Hz, 1H), 2.71 – 2.45

(m, 4H), 2.08 – 2.01 (m, 1H), 1.94 (t, *J* = 7.4 Hz, 2H), 1.49 (p, *J* = 7.0 Hz, 4H), 1.26 (dq, *J* = 8.4, 5.2, 4.4 Hz, 4H) ppm, -C-N*H*-OH signal could not be detected due to solvent exchange. **^{13}C-NMR** (101 MHz, DMSO-d_6, δ): 172.8, 169.9, 169.6, 169.1, 166.9, 166.7, 165.5, 165.4, 155.0, 141.6, 136.9, 133.0, 129.1, 127.9, 120.4, 118.1, 116.8, 116.1, 69.7, 69.7, 69.7, 69.6, 68.8, 67.5, 66.5, 48.8, 40.2*, 38.4, 37.2, 32.2, 31.0, 29.1, 28.4, 26.2, 25.1, 22.0 ppm, * overlapping with DMSO-signal. **HRMS-ESI (*m/z*)**: $[M + Na]^+$ calcd for $C_{38}H_{48}N_6O_{13}$: 819.3172, found: 819.3188. **IR**: $\tilde{\nu}$ = 3261 (br),, 2927 (br), 1773 (w), 1708 (s), 1659 (s), 1531 (m), 1395 (m), 1259 (m), 1099 (m), 1015 (w), 879 (w), 747 (m), 602 (m), 466 (m) cm^{-1}.

4-(1-((2-(2,6-Dioxopiperidin-3-yl)-1,3-dioxoisoindolin-4-yl)oxy)-2-oxo-6,9,12,15-tetraoxa-3-azaoctadecan-18-amido)-*N*-(7-(hydroxyamino)-7-oxoheptyl)benzamide (A4). Synthesized according to general procedure C using **6** (147 mg, 0.10 mmol, 1.00 eq), Fmoc-NH-PEG(4)-OH (146 mg, 0.30 mmol, 3.00 eq), HATU (114 mg, 0.30 mmol, 3.00 equiv.) and DIPEA (70.0 µL, 0.40 mmol, 4.00 equiv.) in DMF (300 µL). The second coupling cycle was performed using the hydroxythalidomide building block **12** (50.0 mg, 0.15 mmol, 1.50 equiv), HATU (76.0 mg, 0.20 mmol, 2.00 equiv.) and DIPEA (52.0 µL, 0.30 mmol, 3.00 equiv.) in DMF (500 µL). Purification by preparative HPLC afforded **A4** as white powder (55.7 mg, 66.2 µmol, 66 %) in >95% purity. **HPLC**: t_R= 13.91 min. **^{1}H-NMR** (400 MHz, DMSO-d_6, δ): 11.11 (s, 1H), 10.32 (s, 1H), 10.12 (s, 1H), 8.29 (t, *J* = 5.6 Hz, 1H), 7.99 (t, *J* = 5.6 Hz, 1H), 7.84 – 7.74 (m, 3H), 7.68 – 7.61 (m, 2H), 7.49 (d, *J* = 7.2 Hz, 1H), 7.39 (d, *J* = 8.5 Hz, 1H), 5.11 (dd, *J* = 12.9, 5.4 Hz, 1H), 4.78 (s, 2H), 3.69* (t, *J* = 6.2 Hz, 2H), 3.56 – 3.38 (m, 14H), 3.31 (q, *J* = 5.7 Hz, 2H), 3.21 (q, *J* = 6.6 Hz, 2H), 2.89 (ddd, *J* = 17.4, 14.1, 5.4 Hz, 1H), 2.70 – 2.45 (m, 4H), 2.12 – 1.98 (m, 1H), 1.93 (t, *J* = 7.3 Hz, 2H), 1.48 (p, *J* = 7.1 Hz, 4H), 1.26 (dq, *J* = 10.0, 5.6 Hz, 4H) ppm, *overlaping with water signal -C-N*H*-OH signal could not be detected due to solvent exchange. **^{13}C-NMR** (101 MHz, DMSO-d_6, δ): 172.8, 169.9, 169.6, 169.1, 166.9, 166.7, 165.5, 165.4, 155.0, 141.6, 136.9, 133.0, 129.1, 127.9, 120.4, 118.1, 116.8, 116.1, 69.8 (2C), 69.7, 69.7 (2C), 69.6, 68.8, 67.5, 66.5, 48.8, 40.1*, 38.4, 37.2, 32.2, 30.9, 29.1, 28.4, 26.2, 25.1, 22.0 ppm, * overlapping with DMSO-signal. **HRMS-ESI (*m/z*)**: $[M + Na]^+$ calcd for $C_{40}H_{52}N_6O_{14}$: 863.3434, found: 863.3449. **IR**: $\tilde{\nu}$ = 3251 (br), 2932 (br), 1774 (w), 1708 (s), 1667 (m), 1615 (m), 1532 (s), 1439 (w), 1397 (m), 1261 (m), 1198 (m), 1110 (m), 1016 (w), 898 (w), 938 (w), 853 (w), 747 (m), 601 (m), 466 (w) cm^{-1}.

4-(1-((2-(2,6-Dioxopiperidin-3-yl)-1,3-dioxoisoindolin-4-yl)amino)-2-oxo-6,9,12,15-tetraoxa-3-azaoctadecan-18-amido)-*N*-(7-(hydroxyamino)-7-oxoheptyl)benzamide (A5). Synthesized according to general procedure C using **6** (147 mg, 0.10 mmol, 1.00 eq), Fmoc-NH-PEG(4)-OH

(146 mg, 0.30 mmol, 3.00 eq), HATU (114 mg, 0.30 mmol, 3.00 equiv.) and DIPEA (70.0 µL, 0.40 mmol, 4.00 equiv.) in DMF (300 µL). The second coupling cycle was performed using the pomalidomide building block **15** (33.1 mg, 0.10 mmol, 1.00 equiv.), HATU (57.0 mg, 0.15 mmol, 1.50 equiv.) and DIPEA (52.0 µL, 0.30 mmol, 3.00 equiv.) in DMF (500 µL). For this coupling a recoupling cycle using the same conditions was needed. Purification by preparative HPLC afforded **A5** as yellow powder (52.1 mg, 62.0 µmol, 62 %) in >95% purity. **HPLC**: t_R= 13.99 min. **^{1}H-NMR** (400 MHz, DMSO-d_6, δ): 11.09 (s, 1H), 10.32 (s, 1H), 10.12 (s, 1H), 8.29 (t, *J* = 5.6 Hz, 1H), 8.15 (t, *J* = 5.6 Hz, 1H), 7.86 – 7.74 (m, 2H), 7.69 – 7.62 (m, 2H), 7.58 (dd, *J* = 8.5, 7.1 Hz, 1H), 7.07 (d, *J* = 7.1 Hz, 1H), 6.94 (s, 1H), 6.86 (d, *J* = 8.6 Hz, 1H), 5.07 (dd, *J* = 12.9, 5.4 Hz, 1H), 3.93 (s, 2H), 3.69 (t, *J* = 6.2 Hz, 2H)*, 3.59 – 3.44 (m, 14H)*, 3.41 (t, *J* = 5.8 Hz, 2H), 3.23 (dq, *J* = 16.4, 6.7, 6.2 Hz, 4H), 2.89 (ddd, *J* = 17.4, 13.9, 5.5 Hz, 1H), 2.57 (t, *J* = 6.1 Hz, 2H), 2.03 (dtd, *J* = 13.0, 6.0, 2.8 Hz, 1H), 1.93 (t, *J* = 7.3 Hz, 2H), 1.57 – 1.39 (m, 4H), 1.36 – 1.14 (m, *J* = 6.4 Hz, 4H) ppm, *overlaping with water signal -C-N*H*-OH signal could not be detected due to solvent exchange. **^{13}C-NMR** (101 MHz, DMSO-d_6, δ): 172.8, 170.1, 169.6, 169.1, 168.7, 168.6, 167.3, 165.6, 145.8, 141.6, 136.2, 132.1, 129.1, 128.0, 118.1, 117.5, 111.0, 109.9, 69.8 (2C), 69.7, 69.7 (2C), 69.6, 68.9, 66.5, 48.6, 45.2, 40.2*, 38.7, 37.2, 32.2, 31.0, 29.1, 28.4, 26.2, 25.1, 22.2 ppm, * overlapping with DMSO-signal. **HRMS-ESI (*m/z*)**: [*M* + Na]$^+$ calcd for $C_{40}H_{53}N_7O_{13}$: 862.3594, found: 862.3596. **IR**: $\tilde{\nu}$ = 3262 (br), 2865 (br), 1757 (w), 1696 (s), 1624 (m), 1528 (m), 1505 (m), 1405 (m), 1359 (m), 1175 (m), 1111 (s), 1022 (w), 931 (w), 853 (w), 814 (w), 747 (m), 595 (w), 521 (w), 467 (w) cm^{-1}.

4-(8-(2-((2-(2,6-Dioxopiperidin-3-yl)-1,3-dioxoisoindolin-4-yl)oxy)acetamido)octanamido)-N-(7-(hydroxyamino)-7-oxoheptyl)benzamide (A6). Synthesized according to general procedure C using **6** (168 mg, 0.15 mmol, 1.00 eq), **8** (172 mg, 0.45 mmol, 3.00 eq), HATU (171 mg, 0.45 mmol, 3.00 equiv.) and DIPEA (105 µL, 0.60 mmol, 4.00 equiv.) in DMF (500 µL). The second coupling cycle was performed using the hydroxythalidomide building block **12** (99.7 mg, 0.30 mmol, 2.00 equiv.), HATU (125 mg, 0.33 mmol, 2.20 equiv.) and DIPEA (92 µL, 0.53 mmol, 3.50 equiv.) in DMF (500 µL). Purification by preparative HPLC afforded **A6** as white powder (49 mg, 66.8 µmol, 45 %) in >95% purity. **HPLC**: t_R= 14.98 min. **^{1}H-NMR** (400 MHz, DMSO-d_6, δ): 11.11 (s, 1H), 10.32 (s, 1H), 10.04 (s, 1H), 8.28 (t, *J* = 5.6 Hz, 1H), 7.92 (t, *J* = 5.7 Hz, 1H), 7.81 (m, 1H), 7.79 – 7.73 (m, 2H), 7.66 – 7.60 (m, 2H), 7.48 (d, *J* = 7.2 Hz, 1H), 7.39 (d, *J* = 8.5 Hz, 1H), 5.12 (dd, *J* = 12.9, 5.4 Hz, 1H), 4.76 (s, 2H), 3.21 (q, *J* = 6.7 Hz, 2H), 3.14 (q, *J* = 6.6 Hz, 2H), 2.90 (ddd, *J* = 17.5, 14.0, 5.4 Hz, 1H), 2.66 – 2.46 (m, 2H), 2.31 (t, *J* = 7.4 Hz, 2H), 2.10 – 1.99 (m, 1H), 1.94 (t, *J* = 7.4 Hz, 2H), 1.58 (t, *J* = 7.1 Hz, 2H), 1.46 (dp, *J* =

20.0, 6.9 Hz, 6H), 1.27 (dd, *J* = 7.1, 3.1 Hz, 10H) ppm, -C-N*H*-OH signal could not be detected due to solvent exchange. **^{13}C-NMR** (101 MHz, DMSO-d_6, δ): 172.8, 171.6, 169.9, 169.1, 166.7, 166.6, 165.6, 165.5, 155.1, 141.7, 136.9, 133.0, 128.9, 127.9, 120.4, 118.1, 116.8, 116.0, 67.7, 48.8, 40.2*, 38.3, 36.4, 32.2, 30.9, 29.1, 29.0, 28.6, 28.5, 28.4, 26.2, 26.2, 25.1, 24.9, 22.0 ppm, *overlapping with DMSO-signal. **HRMS-ESI (*m/z*)**: $[M + Na]^+$ calcd for $C_{37}H_{46}N_6O_{10}$: 757.3168, found: 757.3166. **IR**: $\tilde{\nu}$ = 3262 (br), 2928 (br), 1773 (w), 1708 (s), 1660 (s), 1531 (m), 1484 (w), 1394 (m), 1260 (m), 1198 (m), 1098 (w), 940 (w), 746 (m), 603 (m), 466 (w) cm^{-1}.

***N*-((13S)-1-((2-(2,6-Dioxopiperidin-3-yl)-1,3-dioxoisoindolin-4-yl)oxy)-13-((2-(2-(2-((4-((7-(hydroxyamino)-7-oxoheptyl)carbamoyl)phenyl)amino)-2-oxoethoxy)ethoxy)ethyl)carbamoyl)-2,11-dioxo-6,9-dioxa-3,12-diazaoctadecan-18-yl)-3',6'-dihydroxy-3-oxo-3*H*-spiro[isobenzofuran-1,9'-xanthene]-5-carboxamide (A7).** Synthesized using **6** in a 0.15 mmol scale following standard Fmoc-strategy solid-phase protocol. For the coupling of the PEG-linker, Fmoc-O2Oc-OH (231 mg, 0.60 mmol, 4.00 equiv.), HATU (228 mg, 0.60 mmol, 4.00 equiv.) and DIPEA (131 µL, 0.75 mmol, 5.00 equiv.) were used. For coupling of the fluorescently labeled lysine commercially available Fmoc-L-Lys(5/6FAM) (218 mg, 0.30 mmol, 2.00 equiv.), Oxyma (64.0 mg, 0.45 mmol, 3.00 equiv.) and DIC (70.5 µL, 0.45 mmol, 3.00 equiv.) were used. CRBN ligand coupling was performed using (2-(2,6-dioxopiperidin-3-yl)-1,3-dioxoisoindolin-4-yl)glycine **12** (99.7 mg, 0.30 mmol, 2.00 equiv), HATU (125 mg, 0.33 mmol, 2.20 equiv.) and DIPEA (92.6 µL, 0.53 mmol, 3.50 equiv.). All couplings were performed in DMF (750 µL) for 4 h. Purification by preparative HPLC afforded **A7** as yellow fluorescent powder (106 mg, 77.4 µmol, 52%). An isomer mixture containing 5/6-carboxyfluorescein in a ratio of 0.6:0.4 (determined by ^{1}H-NMR) was isolated as product. The isomer determination was not further evaluated. **A7** was used as mixture of both isomers. **HPLC**: t_R= 14.84. **^{1}H-NMR** (400 MHz, DMSO-d_6, δ): 11.10 (s, 1H), 10.33 (s, 1H), 9.83 (s, 0.6 H), 9.81 (s, 0.4 H), 8.77 (t, *J* = 4.7 Hz, 0.6 H), 8.63 (t, *J* = 4.4 Hz, 0.4 H), 8.43 (s, 0.6 H), 8.31 (t, *J* = 5.5 Hz, 1H), 8.22 (d, *J* = 8.1 Hz, 0.6H), 8.18 – 8.08 (m, 1.4 H), 8.05 (t, *J* = 6.3 Hz, 1.4H), 7.82 – 7.73 (m, 3H), 7.73 – 7.65 (m, 2.4 H), 7.59 (d, *J* = 8.4 Hz, 0.6 H), 7.54 (d, *J* = 8.5 Hz, 0.4 H), 7.47 (dd, *J* = 7.2, 3.5 Hz, 1H), 7.41 – 7.34 (m, 1.6 H), 6.69 (t, *J* = 2.4 Hz, 2H), 6.61 – 6.51 (m, 4H), 5.11 (dd, *J* = 12.8, 5.4 Hz, 1,2 H), 4.80 (s, 1.2 H), 4.78 (s, 0.8 H), 4.37 – 4.26 (m, 2 H), 4.09 (s, 1.2 H), 4.08 (s, 0.8 H), 3.97 – 3.78 (m, 2H), 3.69 – 3.09 (m, 20H), 2.94 – 2.83 (m, 1H), 2.68 – 2.53 (m, 2H), 2.08 – 1.99 (m, 1H), 1.93 (t, *J* = 7.3 Hz, 2H), 1.73 – 1.38 (m, 8H), 1.37 – 1.07 (m, 6H) ppm.**^{13}C-NMR** (101 MHz, DMSO-d_6, δ): 172.8, 171.4, 171.4, 169.9, 169.1, 168.9, 168.9, 168.6, 168.2, 168.1, 166.9, 166.7, 165.5, 165.4, 164.5, 164.3, 159.6, 158.5, 158.1, 155.0, 154.6, 152.7, 151.8,

140.8, 140.7, 136.9, 136.4, 134.7, 133.0, 129.6, 129.4, 129.2, 129.1, 128.1, 127.9, 126.4, 124.8, 124.2, 123.2, 122.2, 120.3, 118.7, 116.8, 116.0, 112.8, 112.7, 109.2, 109.1, 102.3, 83.4, 70.3, 70.3, 70.2, 69.7, 69.7, 69.4, 69.4, 68.9, 67.5, 51.7, 51.6, 48.8, 40.2*, 38.5, 38.4, 32.3, 32.2, 30.9, 29.1, 28.7, 28.6, 28.4, 26.2, 25.1, 22.7, 22.0 ppm, *overlapping with DMSO-signal. **HRMS-ESI (*m/z*)**: [*M* + Na]$^+$ calcd for $C_{68}H_{75}N_9O_{22}$: 1392,4919, found: 1392,4933. **IR**: $\tilde{\nu}$ = 3265 (br), 3095 (br), 2931 (br), 1773 (w), 1708 (s), 1639 (m), 1613 (m), 1531 (s), 1453 (s), 1396 (m), 1300 (m), 1262 (m), 1198 (s), 1116 (s), 1016 (w), 938 (w), 852 (w), 747 (m), 600 (m), 466 (m) cm^{-1}.

4-((5-(1-((2-(2,6-Dioxopiperidin-3-yl)-1,3-dioxoisoindolin-4-yl)oxy)-2-oxo-6,9,12-trioxa-3-azapentadecan-15-amido)-2-methyl-1*H*-benzo[*d*]imidazol-1-yl)methyl)-3-fluoro-*N*-hydroxybenzamide x TFA (B1). Synthesized according to general procedure C using **7** (145 mg, 90.0 µmol, 1.00 eq), Fmoc-NH-PEG(3)-OH (120 mg, 0.27 mmol, 3.00 eq), HATU (103 mg, 0.27 mmol, 3.00 equiv.) and DIPEA (64.0 µL, 0.36 mmol, 4.00 equiv.) in DMF (300 µL). The second coupling cycle was performed using the hydroxythalidomide building block **12** (44.9 mg, 135 µmol, 1.50 equiv.), HATU (68.4 mg, 0.18 mmol, 2.00 equiv.) and DIPEA (46.8 µL, 0.27 mmol, 3.00 equiv.) in DMF (300 µL). Purification by preparative HPLC afforded **B1** as colorless TFA salt (58.0 mg, 61.3 µmol, 68%) in >95% purity. **HPLC**: t_R= 13.07. **^{1}H-NMR** (400 MHz, DMSO-d_6, δ): 11.35 (s, 1H), 11.11 (s, 1H), 10.29 (s, 1H), 8.29 (d, *J* = 1.9 Hz, 1H), 7.99 (t, *J* = 5.7 Hz, 1H), 7.80 (dd, *J* = 8.5, 7.3 Hz, 1H), 7.69 (d, *J* = 9.0 Hz, 1H), 7.64 – 7.55 (m, 2H), 7.52 – 7.44 (m, 2H), 7.38 (dt, *J* = 7.8, 3.6 Hz, 2H), 5.77 (s, 2H), 5.11 (dd, *J* = 12.9, 5.4 Hz, 1H), 4.78 (s, 2H), 3.70 (t, *J* = 6.2 Hz, 2H), 3.49 (dt, *J* = 6.4, 2.0 Hz, 8H), 3.43 (t, *J* = 5.7 Hz, 2H), 3.28 (q, *J* = 5.7 Hz, 2H), 2.89 (ddd, *J* = 17.4, 14.0, 5.4 Hz, 1H), 2.81 (s, 3H), 2.69 – 2.52 (m, 4H), 2.08 – 1.99 (m, 1H) ppm, -C-N*H*-OH signal could not be detected due to solvent exchange. **^{19}F-NMR** (282 MHz, DMSO-d_6, δ): □74.10 (s, TFA), □115.73 (s) ppm. **^{13}C-NMR** (101 MHz, DMSO-d_6, δ): 172.7, 169.8, 169.7, 166.9, 166.7, 165.4, 159.8 (d, $^1J_{C\text{-}F}$ = 247.2 Hz), 158.2, 157.9, 154.9, 152.0, 137.2, 136.9, 135.1 (d, $^3J_{C\text{-}F}$ = 7.5 Hz), 133.0, 129.8 (d, $^3J_{C\text{-}F}$ = 3.2 Hz), 127.8, 124.3 (d, $^2J_{C\text{-}F}$ = 14.6 Hz), 123.2 (d, $^4J_{C\text{-}F}$ = 2.6 Hz), 120.3, 117.4, 116.7, 116.6 (q, $^1J_{C\text{-}F}$ = 295.9 Hz, TFA), 116.0, 114.2 (d, $^2J_{C\text{-}F}$ = 22.8 Hz), 112.8, 103.7, 69.7, 69.7, 69.7, 69.6, 68.8, 67.5, 66.5, 48.8, 42.4 (d, ^3J = 2.7 Hz), *, 38.4, 37.2, 30.9, 22.0, 11.9 ppm, *overlapping with DMSO-signal. **HRMS-ESI (*m/z*)**: [*M* + Na]$^+$ calcd for $C_{40}H_{42}FN_7O_{12}$: 854.2768, found: 854.2788. **IR**: $\tilde{\nu}$ = 2872 (br), 1711 (s), 1667 (m), 1553 (w), 1485 (w), 1394 (m), 1355 (w), 1263 (w), 1199 (s), 1124 (m), 880 (w), 748 (m), 603 (w), 527 (w), 467 (w) cm^{-1}.

4-((5-(1-((2-(2,6-Dioxopiperidin-3-yl)-1,3-dioxoisoindolin-4-yl)oxy)-2-oxo-6,9,12,15-tetraoxa-3-azaoctadecan-18-amido)-2-methyl-1*H*-benzo[*d*]imidazol-1-yl)methyl)-3-fluoro-*N*-hydroxybenzamide x TFA (B2). Synthesized according to general procedure C using **7** (167 mg, 0.10 mmol, 1.00 eq), Fmoc-NH-PEG(4)-OH (146 mg, 0.30 mmol, 3.00 eq), HATU (114 mg, 0.30 mmol, 3.00 equiv.) and DIPEA (70.0 µL, 0.40 mmol, 4.00 equiv.) in DMF (550 µL). The second coupling cycle was performed using the hydroxythalidomide building block **12** (45.0 mg, 0.14 mmol, 1.35 equiv), HATU (76.0 mg, 0.20 mmol, 2.00 equiv.) and DIPEA (52.0 µL, 0.30 mmol, 3.00 equiv.) in DMF (550 µL). Purification by preparative HPLC afforded **B2** as colorless TFA salt (61.2 mg, 61.8 µmol, 62%) in >95% purity. **HPLC**: t_R= 13.18. **^{1}H-NMR** (400 MHz, DMSO-d_6, δ): 11.36 (s, 1H), 11.11 (s, 1H), 10.31 (s, 1H), 8.29 (d, *J* = 1.9 Hz, 1H), 8.00 (t, *J* = 5.6 Hz, 1H), 7.80 (dd, *J* = 8.5, 7.3 Hz, 1H), 7.70 (d, *J* = 9.0 Hz, 1H), 7.64 – 7.55 (m, 2H), 7.52 – 7.46 (m, 2H), 7.44 – 7.36 (m, 2H), 5.77 (s, 2H), 5.11 (dd, *J* = 12.9, 5.4 Hz, 1H), 4.78 (s, 2H), 3.71 (t, *J* = 6.2 Hz, 2H), 3.57 – 3.38 (m, 14H), 3.30 (q, *J* = 5.7 Hz, 2H), 2.89 (ddd, *J* = 17.8, 14.2, 5.6 Hz, 1H), 2.82 (s, 3H), 2.70 – 2.51 (m, 4H), 2.07 – 1.97 (m, 1H) ppm, -C-N*H*-OH signal could not be detected due to solvent exchange. **^{19}F-NMR** (376 MHz, DMSO-d_6, δ): -74.17 (s, TFA), -115.72 (dd, *J* = 10.9, 7.7 Hz) ppm.**^{13}C-NMR** (101 MHz, DMSO-d_6, δ): 172.8, 169.9, 169.7, 166.9, 166.7, 165.4, 159.8 (d, $^1J_{C\text{-}F}$ = 247.3 Hz), 158.2, 157.9, 155.0, 152.0, 137.2, 136.9, 135.1 (d, $^3J_{C\text{-}F}$ = 7.3 Hz), 133.0, 129.8 (d, $^3J_{C\text{-}F}$ = 3.0 Hz), 127.8, 124.3 (d, $^2J_{C\text{-}F}$ = 14.7 Hz), 123.2, 120.3, 117.4, 116.8, 116.5 (q, $^1J_{C\text{-}F}$ = 296.6 Hz, TFA) 116.1, 114.1 (d, $^2J_{C\text{-}F}$ = 22.7 Hz), 112.8, 103.7, 69.8 (2C), 69.7, 69.7, 69.6, 68.8, 67.5, 66.5, 48.8, 42.4, *, 38.4, 37.2, 30.9, 22.0, 12.0 ppm, *overlapping with DMSO-signal. **HRMS-ESI (*m/z*)**: [*M* + Na]$^+$ calcd for $C_{42}H_{46}FN_7O_{13}$: 898.3030, found: 898.3021. **IR**: $\tilde{\nu}$ = 3221 (br), 3094 (br), 2872 (br), 1773 (w), 1709(s), 1667 (s), 1554 (w), 1501 (w), 1485 (m), 1394 (m), 1262 (m), 1197 (s), 1121 (s), 1056 (m), 939 (w), 879 (w), 834 (m), 818 (m), 748 (m), 719 (m), 674 (w), 602 (m), 628 (w), 466 (m) cm^{-1}.

4-((5-(1-((2-(2,6-Dioxopiperidin-3-yl)-1,3-dioxoisoindolin-4-yl)amino)-2-oxo-6,9,12,15-tetraoxa-3-azaoctadecan-18-amido)-2-methyl-1*H*-benzo[*d*]imidazol-1-yl)methyl)-3-fluoro-*N*-hydroxybenzamide x TFA (B3). Synthesized according to general procedure C using **7** (167 mg, 0.10 mmol, 1.00 eq), Fmoc-NH-PEG(4)-OH (146 mg, 0.30 mmol, 3.00 eq), HATU (114 mg, 0.30 mmol, 3.00 equiv.), and DIPEA (70.0 µL, 0.40 mmol, 4.00 equiv.) in DMF (550 µL). The second coupling cycle was performed using the pomalidomide building block **15** (49.0 mg, 0.15 mmol, 1.50 equiv.), HATU (76.0 mg, 0.20 mmol, 2.00 equiv.) DIPEA (52.0 µL, 0.30 mmol, 3.00 equiv.) in DMF (550 µL). Purification by preparative HPLC afforded **B3** as yellow TFA salt (69.7 mg, 70.5 µmol, 71%) in >95%

purity. **HPLC**: t_R= 13.22. **^{1}H-NMR** (400 MHz, DMSO-d_6, δ): 11.35 (s, 1H), 11.10 (s, 1H), 10.29 (s, 1H), 8.28 (d, *J* = 1.8 Hz, 1H), 8.15 (t, *J* = 5.6 Hz, 1H), 7.69 (d, *J* = 9.0 Hz, 1H), 7.64 – 7.54 (m, 3H), 7.47 (dd, *J* = 9.0, 1.9 Hz, 1H), 7.38 (t, *J* = 7.9 Hz, 1H), 7.06 (d, *J* = 7.0 Hz, 1H), 6.94 (s, 1H), 6.85 (d, *J* = 8.5 Hz, 1H), 5.76 (s, 2H), 5.07 (dd, *J* = 12.7, 5.4 Hz, 1H), 3.93 (d, *J* = 4.5 Hz, 2H), 3.71 (t, *J* = 6.2 Hz, 2H)*, 3.53 – 3.43 (m, 12H)*, 3.40 (t, *J* = 5.8 Hz, 2H)*, 3.24 (q, *J* = 5.7 Hz, 2H), 2.97 – 2.85 (m, 1H), 2.80 (s, 3H), 2.65 – 2.42 (m, 3H)**, 2.08 – 1.98 (m, 2H) ppm, *overlapping with water signal,**overlapping with DMSO-signal, -C-N*H*-OH signal could not be detected due to solvent exchange. **^{19}F-NMR** (376 MHz, DMSO-d_6, δ): -74.03 (s, TFA), -115.73 t, *J* = 8.4 Hz) ppm. **^{13}C-NMR** (101 MHz, DMSO-d_6, δ): 172.8, 170.0, 169.7, 168.7, 168.6, 167.3, 159.8 (d, $^1J_{C\text{-}F}$ = 247.2 Hz), 158.3, 158.0, 152.0, 145.8, 137.2, 136.2, 135.1 (d, $^3J_{C\text{-}F}$ = 7.1 Hz), 132.0, 129.8 (d, $^3J_{C\text{-}F}$ = 2.8 Hz), 127.9, 124.4 (d, $^2J_{C\text{-}F}$ = 14.6 Hz), 123.3 (d, $^4J_{C\text{-}F}$ = 2.2 Hz), 117.5, 117.4, 116.7 (q, $^1J_{C\text{-}F}$ = 297.1 Hz, TFA), 114.2 (d, $^2J_{C\text{-}F}$ = 23.0 Hz), 112.7, 111.0, 109.8, 103.8, 69.8 (2C), 69.7, 69.7, 69.6, 68.9, 66.5, 48.6, 45.2, 42.4 (d, $^3J_{C\text{-}F}$ = 2.6 Hz), 40.2*, 38.6, 37.2, 31.0, 22.2, 12.0 ppm, *overlapping with DMSO-signal. **HRMS-ESI (*m/z*)**: [*M* + Na]$^+$ calcd for $C_{42}H_{47}FN_8O_{12}$: 897.3190, found: 897.3168. **IR**: $\tilde{\nu}$ = 2872 (br), 1695 (s), 1624 (m), 1554 (w), 1502 (m), 1407 (m), 1360 (m), 1322 (w), 1260 (m), 1199 (s), 1115 (m), 1024 (w), 880 (w), 814 (m), 747 (m), 719 (m), 677 (w), 602 (m), 525 (w), 468 (w) cm^{-1}.

4-((5-(8-(2-((2-(2,6-Dioxopiperidin-3-yl)-1,3-dioxoisoindolin-4-yl)oxy)acetamido)octanamido)-2-methyl-1*H*-benzo[*d*]imidazol-1-yl)methyl)-3-fluoro-*N*-hydroxybenzamide (B4). Synthesized according to general procedure C using **7** (167 mg, 0.10 mmol, 1.00 eq), **8** (153 mg, 0.40 mmol, 4.00 eq), HATU (152 mg, 0.40 mmol, 4.00 equiv.) and DIPEA (87.5 µL, 0.50 mmol, 5.00 equiv.) in DMF (600 µL). The second coupling cycle was performed using the hydroxythalidomide building block **12** (66.0 mg, 0.20 mmol, 2.00 equiv), HATU (84.0 mg, 0.22 mmol, 2.20 equiv.) and DIPEA (61.1 µL, 0.35 mmol, 3.50 equiv.) in DMF (600 µL). For this coupling step a recoupling cycle using the same amounts of reagents in a mixture of DMF/CH_2Cl_2 (600 µL, 1:1) was needed. Purification by preparative HPLC afforded **B4** as white powder (24.0 mg, 27.2 µmol, 27%) in >95% purity. **HPLC**: t_R= 14.01. **^{1}H-NMR** (400 MHz, DMSO-d_6, δ): 11.35 (s, 1H), 11.11 (s, 1H), 10.22 (s, 1H), 8.28 (d, *J* = 1.9 Hz, 1H), 7.93 (t, *J* = 5.7 Hz, 1H), 7.80 (dd, *J* = 8.5, 7.3 Hz, 1H), 7.68 (d, *J* = 9.0 Hz, 1H), 7.65 – 7.55 (m, 2H), 7.52 – 7.43 (m, 2H), 7.39 (d, *J* = 8.3 Hz, 2H), 5.77 (s, 2H), 5.11 (dd, *J* = 12.8, 5.4 Hz, 1H), 4.76 (s, 2H), 3.14 (q, *J* = 6.6 Hz, 2H), 2.97 – 2.82 (m, 1H), 2.81 (s, 3H), 2.69 – 2.53 (m, 2H), 2.33 (t, *J* = 7.4 Hz, 2H), 2.10 – 1.98 (m, 1H), 1.59 (t, *J* = 7.1 Hz, 2H), 1.44 (t, *J* = 6.9 Hz, 2H), 1.34 – 1.20 (m, 6H) ppm, -C-N*H*-OH signal could not be detected due to solvent exchange. **^{19}F-NMR** (377 MHz, DMSO-d_6, δ): -73.20 (s,

TFA), -114.91 (t, J = 9.1 Hz) ppm.**^{13}C-NMR** (101 MHz, DMSO-d_6, δ): 172.8, 171.7, 169.9, 166.7, 166.6, 165.5, 159.8 (d, $^{1}J_{C\text{-}F}$ = 247.0 Hz), 158.2, 157.9, 155.0, 151.9, 137.4, 136.9, 135.1 (d, $^{3}J_{C\text{-}F}$ = 7.1 Hz), 133.0, 129.8 (d, $^{3}J_{C\text{-}F}$ = 3.0 Hz), 127.7, 124.4 (d, $^{2}J_{C\text{-}F}$ = 14.3 Hz), 123.2 (d, $^{4}J_{C\text{-}F}$ = 2.5 Hz), 120.4, 117.4, 116.8, 116.6 (q, $^{1}J_{C\text{-}F}$ = 297.5, Hz, TFA), 116.0, 114.2 (d, $^{2}J_{C\text{-}F}$ = 22.7 Hz), 112.7, 103.7, 67.7, 48.8, 42.4 (d, $^{3}J_{C\text{-}F}$ = 3.0 Hz), 38.3, 36.4, 30.9, 29.0, 28.6, 28.5, 26.2, 25.0, 22.0, 12.0 ppm. **HRMS-ESI (*m/z*)**: $[M + Na]^+$ calcd for $C_{39}H_{40}FN_7O_9$: 792.2764, found: 792.2754. **IR**: $\tilde{\nu}$ = 3226 (br), 2933 (br), 2859 (br), 1709 (s), 1666 (s), 1555 (m), 1486 (m), 1395 (m), 1323 (w), 1298 (w), 1263 (m), 1198 (s), 1124 (m), 1286 (w), 1018 (w), 942 (w), 825 (w), 746 (m), 720 (m), 676 (m), 663 (w), 604 (m), 567 (w), 528 (w), 468 (m) cm^{-1}.

In vitro human HDAC1 and HDAC6 assay

In vitro inhibitory activities against HDAC1 and HDAC6 were measured using a previously published protocol.[55] OptiPlate-96 black microplates (Perkin Elmer) were used with an assay volume of 50 µL. 5 µL test compound or control, diluted in assay buffer (50 mM Tris-HCl, pH 8.0, 137 mM NaCl, 2.7 mM KCl, 1 mM $MgCl_2$, 0.1 mg/mL BSA), were incubated with 35 µL of the fluorogenic substrate ZMAL (Z-Lys(Ac)-AMC) (21.43 µM in assay buffer) and 10 µL of human recombinant HDAC1 (BPS Bioscience, Catalog# 50051) or HDAC6 (BPS Bioscience, Catalog# 50006) at 37 °C. After an incubation time of 90 min, 50 µL of 0.4 mg/mL trypsin in trypsin buffer (50 mM Tris-HCl, pH 8.0, 100 mM NaCl) were added, followed by further incubation at 37 °C for 30 min. Fluorescence was measured with an excitation wavelength of 355 nm and an emission wavelength of 460 nm using a Fluoroskan Ascent microplate reader (Thermo Scientific). All compounds were tested at least twice and in duplicates and the 50% inhibitory concentration (IC_{50}) was determined by plotting dose response curves and nonlinear regression with GraphPad Prism.

Cell culture

The leukemic cell lines HL-60, MOLM-13, MV4-11, THP-1, KASUMI-1 (AML); 697, REH (B-ALL) and K562 (CML) were cultured in RPMI 1640 GlutaMax (Life Technology, California, USA, Catalog #61870036) supplemented with 10 – 20 % FCS. SKNO-1(AML) were cultured in RPMI 1640 GlutaMax supplemented with 10% FCS and 10 ng/ml GM-CSF. All cells were cultured in a 37 °C humidified incubator with 5% CO_2 according to the suggested culture conditions from DSMZ

(https://www.dsmz.de), with the addition of 1% penicillin-streptomycin (Catalog #15070063, Life Technologies, CA, USA,).

Cell viability assay

The cell viability assay was performed to determine the IC_{50} values for the leukemic cell lines. The experimental compounds, vorinostat (Catalog #S1047) and nexturastat A (Catalog #S1047, Selleckchem, Houston, USA) were first dissolved in DMSO with an initial stock concentration of 10 mM and printed on white 384-well plates (Catalog #3570, Thermo Fisher Scientific, MA, USA) with increasing concentrations (0.5 µM – 50 µM) by using a digital dispenser (D300e, Tecan, Männedorf, Switzerland). Afterwards, 30 µl of cell suspension/well were seeded with a concentration of 0.04 x 10^6 cells /mL and incubated under standard culture conditions. After 72 h the cell viability was measured utilizing the ATP based CellTiter-Glo luminescent assay (Promega, WI, USA, Catalog #G7573) with a microplate reader (Spark, Tecan). The obtained raw data were normalised to DMSO treated controls (DMSO < 0.5%) and the IC_{50} values calculated using the sigmoid dose curve (Hill slope) and nonlinear regression (GraphPad Prism Inc., CA, USA) (n=3). The IC_{50} data were plotted as a clustered heat map, followed by unsupervised hierarchical clustering. Each box of the heatmap represents the mean of three independent experiments (n=3). The average IC_{50} values of across all tested cell lines were used for statistical analysis, *, ** and n.s. indicate significant one-way ANOVA P values of < 0.05, < 0.01 and > 0.05, respectively. The IC_{50} values $\pm$ SD that were used for statistical analysis.

Immunoblot

Cells (0.5 x 10^6 cells/mL) were treated with the indicated concentration of the compound or vehicle (DMSO) for 6 h or 24 h under standard culture conditions. Cell pellets were lysed with 300 µL RIPA buffer (50 mM Tris-HCl pH 8.0, 1 % Triton X-100, 0.5 % sodium deoxycholate, 0.1% SDS, 150 mM sodium chloride, 2 mM EDTA, supplemented with protease inhibitors (Roche, Switzerland, Catalog #11697498001) and phosphatase inhibitor (Roche, Switzerland, Catalog #4906845001) cocktail tablets, Thermo Scientific, Wesel, Germany) according to manufactures guidelines. After centrifugation, the protein concentration of the whole cell extracts was determined using the Pierce BCA protein assay kit (Catalog #23225, ThermoFisher Scientific, MA, USA), according to manufacturer's guidelines. 20 µg of total protein extracts were resolved by a 8% or 12% SDS-PAGE at 60 mA for 60 min and transferred at 100 V for 60 min~120 min to nitrocellulose blotting membrane (Catalog #10600002, GE Healthcare, Germany) utilizing the wet mini trans-blot electrophoretic transfer cell system

(Catalog #1703930. Bio-Rad, CA, USA,). PageRuler Prestained Protein Ladder, 10 to 180 kDa (Catalog #26616, ThermoFisher Scientific) was used as protein molecular weight marker. First, blots were incubated in 5% BSA in TBS-T blocking solution for 30 min under slight agitation at room temperature, followed by washing three times (5 min) with TBS-T. Afterwards, the blots were incubated over night at 4°C with anti-HDAC6 (Catalog #7558), anti-HDAC1 (Catalog #5356), anti-HDAC4 (Catalog #2072), anti-α-tubulin (Catalog #2144), anti-acetyl-α-tubulin (Catalog #5335), anti-histone H3 (Catalog #4499), anti-acetyl-histone H3 (Catalog #9677) and anti-GAPDH (Catalog #5174) antibodies (Cell Signaling Technology, MA, USA). All primary antibodies were diluted 1:1000 in 5% BSA/ TBS-T. Afterwards, blots were washed three times for 5 min in TBS-T. Next, blots were incubated with 1:2000 dilution of secondary horseradish peroxidase-conjugated antibodies (Catalog #7074, Cell Signalling Technology) for 2 h at room temperature. Blots were washed three times with TBS-T and developed with the ECL system (Catalog #GERPN2109, GE Healthcare, IL, USA), following manufacturer's guidelines. Blots were detected and analysed with the Jess western blot system (Protein simple, CA, USA).

Generation of HDAC6-HiBiT knockin clones

The generation of HiBit-HDAC6 knock in cells (K562) was performed following this published protocol[47], with minor adaptions. See Table S5, Supporting information for crRNA and repair template (single-stranded oligodeoxynucleotide or ssODN) sequences.

a) Labeling of single-stranded oligodeoxynucleotide (ssODN)

Labeling of the donor DNA was carried out using LabelIT MFP488 Nucleic Acid Labeling Kit (Catalog #MIR7125; Mirus Bio, WI, USA) according to the manufacturer's instructions. DNase- and RNase free water, 10X labeling buffer A, ssODN (1 mg/mL) and 1:10 of labelIT Reagent was mixed and incubated at 37°C for 1 h while centrifuging briefly after 30 min. Purification was conducted using G50 microspin columns. To this end, the total volume of 50 µL was slowly applied to the top center of the resin and centrifuged (700 x g, 2 min). Afterwards, the purified sample was obtained and stored at -20 °C.

b) Transfection of cells with CRISPR/Cas9-gRNA RNP complex

Transfection was carried out using the Amaxa Nucleofection system (SF Cell Line Kit, Catalog# V4XC-2032). For 2 X 10^5 K562 cells, 100 pmol of Cas9 protein (Alt-R S.p. HiFi Cas9 nuclease V3, Catalog# 1081060; IDT, IA, USA) was mixed with 120 pmol of gRNA (crRNA:tracrRNA 1:1) and assembled for 20 min at room temperature. Afterwards, the labeled ssODN was added and the mixture was combined

with the cell suspension (resuspended cells in Nucleofector solution SF) and the electroporation enhancer. The complete volume was gently transferred to the nucleocuvette module, placed in the 4D-Nucleofector system and electroporated with the program 'CA-137'. Pre-warmed culture media was quickly added to the cells and transferred to a 96 well plate.

c) Generation of monoclonal cells

The generation of monoclonal cells was done via semi-solid cloning. The cells were seeded (100 cells/mL) in methylcellulose medium for human cells (MethoCult™ H4100 STEMCELL, Catalog #04100) supplemented with FCS (Sigma-Aldrich, St. Louis, MO, USA) and penicillin/streptomycin (Invitrogen, Carlsbad, CA, USA). After 10 days, the colonies were picked and transferred to a 96 well plate.

d) Validate editing event in cells

Nano-Glo® HiBiT Lytic Detection System (Catalog #N3030; Promega) was used to select positive clones. Briefly, 2 x 10^4 cells were taken 48 h post-electroporation and mixed 1:1 with Nano-Glo® HiBiT Lytic Reagent (LgBiT Protein 1:100 and Nano-Glo® HiBiT Lytic Substrate 1:50 in Nano-Glo® HiBiT Lytic Buffer). The mixture was incubated 10 min at room temperature and luminescence was measured using Tecan Spark microplate reader. The background luminescence was measured using unedited cells and was subtracted from all readings. Later to ensure that the selected colonies are positive for the HiBiT constructs at the genomic (DNA) level and to omit any off target activity following Crispr-Cas9 editing, sanger sequencing was performed by designing the primers (For: 5'-cttgtggggactgtggaaca-3' and Rev 5'-aggataacattggcgggagg-3') spanning the donor template region. The clone (s) without any variations/mutations (SNPs, insertions or deletions) were picked for the further degradation assay.

HDAC6-HiBiT PROTAC degradation assay

A validated HDAC6-HiBiT tagged monoclonal K562 cells were seeded (0.2 x 10^6 per mL) in FCS free media on 12 well cell culture plates. Compound was added into the seeding solution at a concentration of 1 µM and DMSO was used as a vehicle control. For every time point of measurement and condition one well was filled with 1 mL of seeding culture. The first measurement was performed after 30 minutes, followed by seven consecutive measurements every hour and a final measurement at 24 hours. Prior to each measurement, the cell culture plate was taken out of the incubator to acclimate to room temperature. Out of each well three times 100 µL were added to a white bottom Thermo Scientiffic Nunclon Delta Surface 96 well plate. Nano-Glo® HiBiT Lytic (100 µL) reagent (LgBiT Protein 1:100 and Nano-Glo® HiBiT Lytic Substrate 1:50 in Nano-Glo® HiBiT Lytic Buffer) was later added to these wells

(Promega). After 10 min of incubation at room temperature the luminescence was measured with a Tecan Spark microplate reader. The luminescence signal of the treated cells was normalized to the DMSO signal.

Mass spectrometry

a) Sample preparation

K562 cells were lysed after 6 h treatment with **A6** or **B4** at 1 µM. Proteins were extracted from frozen cell pellets as described elsewhere.[56] Briefly, cells were lysed and homogenized in urea buffer using a TissueLyser (Qiagen) and, after centrifugation (15 min, 16000 rcf, 4°C), supernatants were collected. After determination of protein concentration (Pierce 660 nm Protein Assay, Thermo Fischer Scientific), samples were adjusted to 0.5 mg/mL total protein concentration with SDS buffer (final 7.5% glycerol, 3% SDS, 37.5 mM Tris/HCl pH 7.0) and 10 µL were reduced (20 mM dithiothreitol, 20 min, 56 °C), alkylated (80 mM iodoacetamide, 15 min, RT, protected from light) and finally underwent tryptic digestion (200 ng trypsin in 50 mM triethylammonium bicarbonate) after applying a slightly modified sp3 protocol[57] using 50 µg 1:1 mix Sera-Mag SpeedBeads. 20% of the peptides were dissolved in 0.1% trifluoracetic acid and subjected to LC-MS analysis.

b) LC-MS analysis

For the LC-MS analysis, a Q Exactive Plus Hybrid Quadrupole-Orbitrap Mass Spectrometer (Thermo Fisher Scientific), operated in positive mode and coupled with a nano electrospray ionization source connected with an Ultimate 3000 Rapid Separation liquid chromatography system (Dionex / Thermo Fisher Scientific, Idstein, Germany) equipped with an Acclaim PepMap 100 C18 column (75 µm inner diameter, 25 cm length, 2 mm particle size from Thermo Fisher Scientific) was applied using a 120 min LC gradient. Capillary temperature was set to 250 °C and source voltage to 1.4 kV. MS survey scans had a mass range from 350 to 2000 m/z at a resolution of 140,000. The automatic gain control was set to 3,000,000 and the maximum fill time was 80 ms. The ten most intensive peptide ions were isolated and fragmented by high-energy collision dissociation.

c) Data analysis

MaxQuant (version 2.0.3.0, Max Planck Institute for Biochemistry, Planegg, Germany) was used for peptide / protein identification and quantification employing a human sequence database (UniProtKB, downloaded on 01/27/2021, 75777 entries). Methionine oxidation and N-terminal acetylation as well as a carbamidomethylation at cysteine residues were considered as variable and fixed modifications,

respectively. A false discovery rate of 1% on protein and peptide level was set as identification threshold. Statistical analysis was performed based on experiment-pairwise median log2(fold change) normalized MaxQuant protein group intensities and LFQ intensities using the "R" (v4.0.4) programming language after removing potential contaminants, reverse hits and proteins only identified by modified peptides. Principal component analysis (PCA) was performed using the prcomp() function and cluster analysis using the heatmap() function with ward.D2 as the hclust method on protein groups with a complete set of valid values over all samples. Testing for significant protein up- or downregulation in differential analyses (**A6** vs. DMSO or **B4** vs. DMSO) was performed using the 'Significance Analysis of Microarrays' (SAM) analysis method[58] within the siggenes package. For this approach, a minimum of four valid values had to be present in at least one group (PROTAC treated or untreated), data were log2 transformed to reach a normal distribution like data structure, and missing values were filled in with random values from sample wise downshifted normal distributions (0.3 s.d. width, 1.8 s.d. downshift). Even at very high permutation based false discovery rate (FDR) settings of up to 50%, no statistically significant proteins were identified.

Simple western immunoassay

Fluorescent (5X) master mix, DTT and biotinylated ladder were prepared as per manufacturer's instruction (BioTechne). 0.40 µg/µL sample per well was prepared by dilution of sample in 0.1x sample buffer and mixing it 5:1 with fluorescent 5x master mix. Incubation for 5 min at 95°C in a PCR cycler (GeneAMP PCR System2700, Applied Biosystems, MA, USA) assures proper protein denaturation. After loading and centrifugation (5 min at 1000 x g at room temperature) of the assay plate, a 12-230 kDA separation module with 25 cartridges (SM-W004, Bio-Techne, MN, USA) was used for the immune assay (JESS, Bio-Techne – ProteinSimple, MN, USA). Conditions include separation for 25 min at 375 V, blocking for 5 min with antibody diluent 2, 30 min incubation with primary antibody and 30 min incubation with secondary antibody. Primary antibody multiplex mix consisted of 1:50 anti-HDAC6 (Catalog #7558), 1:50 anti-GAPDH (Catalog #5174, Cell Signaling Technology) and 1:50 anti-β-actin (Catalog #MAB8929, R&D Systems, MN, USA) was diluted in Antibody Diluent 2. Signals were detected using an anti-rabbit detection module of JESS (Catalog #DM-001, BioTechne), multiplexed with an anti-mouse secondary NIR antibody (Catalog #043-821, BioTechne). Protein levels are calculated by area under the curves of electropherogramms. HDAC6 levels were normalized to the vehicle set to 100% whereas ac-α-tubulin levels were normalized to ac-α-tubulin levels after DMSO treatment set to 0% and maximum protein level set to 100%. DC_{50} was calculated via non-linear regression (log(inhibitor) vs.

response (three paramters)). The non-linear regression was used to generate D_{max} values by subtraction of 100% protein level by “bottom – best-fit value” (GraphPadPrism). EC_{50} of α-tubulin hyper acetylation was calculated via non-linear regression (log(agonist) vs. normalized response – variable slope). Average DC_{50}, D_{max} and EC_{50} values were calculated from three independent simple western immunoassay runs on the treated samples generated from two independent biological replicates.

Caspase 3/7 assay

Cells (0.04 x 10^6 cells/mL) were treated with the indicated concentration of the compounds or vehicle (DMSO) for 48 h under standard culture conditions. Then cells were transferred to white 96-well plates and incubated with Caspase-Glo® 3/7 Substrate (Catalog #G8091, Promega) for 30 min at room temperature, later enzymatic activity of caspase 3/7 was examined by using Caspase-Glo® 3/7 assay (absorbance at 405 nm), following manufacturer’s instructions (Promega) using a microplate reader (Spark, Tecan). The average luminescence values (n=3) of each condition was used for statistical analysis, *, ** and n.s. indicate significant one-way ANOVA P values of < 0.05, < 0.01 and > 0.05 respectively. The IC_{50} values $\pm$ SD that were used for statistical analysis.

Annexin V/Propidium Idodide (PI) apoptosis assay

Cells (0.04 x 10^6 cells/mL) were treated with the indicated concentration of the compound or vehicle (DMSO) for 48 h under standard culture conditions. Cell pellets were washed in ice-cold PBS for once and resuspended in 100 µL Annexin-PI staining solution (containing 1.25 µL Annexin and 2.5 µL PI; FITC Annexin V Apoptosis Detection Kit with PI), Catalog #640914, Biolegend, CA, USA. Following incubation at room temperature for 15 min in the dark, cells were analyzed using a flow cytometer (Beckman Coulter, USA). This allows for the discrimination of live cells (unstained with either fluorochrome) from apoptotic cells (stained only with Annexin V) and necrotic cells (stained with both Annexin V and PI). The average percentage (n=3) of the stained or unstained cells across different conditions was used for statistical analysis, *, ** and n.s. indicate significant one-way ANOVA P values of < 0.05, < 0.01 and > 0.05 respectively.

Cell cycle analysis

Cells (0.04 x 10^6 cells/mL) were treated with the indicated concentration of the compound or vehicle (DMSO) for 48 h under standard culture conditions. Cell pellets were washed in ice-cold PBS for twice and resuspended in 150 µL staining solution containing 0.1% sodium citrate, 0.1% Triton X-100, 50

µg/mL propidium iodide (Tri-sodium citrate 2-hydrate, Catalog #3580.1; Triton X-100, Roth, Germany, Catalog #3051.3; Propidium iodide, Invitrogen, MA, USA, Catalog #P3566). Following incubation at room temperature for 15 min in the dark, cells were analyzed using a flow cytometer (Beckman Coulter, USA). The average percentage of the cells in different cell cycle phase (n=3) was used for statistical analysis, *, ** and n.s. indicate significant one-way ANOVA P values of < 0.05, < 0.01 and > 0.05 respectively.

Immunofluorescence

The Lab-Tek II chamber slide w/Cover RS Glass slides (Nalgene Nunc International, Catalog #154534) were chosen for this experiment, and were coated with a 50 µg/mL solution of Poly-D-Lysine or PDL (Gibco, ThermoFisher Scientific, Catalog #A3890401) and incubated for 7 min - 24 h at 37 °C. All wells treated with PDL were washed three times with PBS, before adding cells. Treated cells were resuspended and centrifuged at 400 x g for 5 min, then resuspended in 1 mL of Dulbecco's phosphor-buffered saline (PBS) (Catalog #D8537-500ML, Sigma-Aldrich, MO, USA). Of the 1 mL cell mix, 400 µL - 500 µL of volume was added to each corresponding well. The micro slides were then placed in the incubator for 30-60 min. After incubation, the slides were observed under a brightfield microscope (magn. 10X) to identify cell attachment to the bottom of the slide. If sufficient cells were attached (~50% confluency), all remaining cell media were removed and 200-300 µL of PBS was added. For fixation, PBS was removed and 200 µL 4% formaldehyde (FA) (VWR PROLABO CHEMICAL, catalog#9713.1000) was added to each well for 10 min at room temperature. A sufficient volume of 1xTBS (10XTBS: 100 mL 1 M Tris (pH7.5), 1400 mM NaCl, (in H_2O), 1xTBS is a 1:10 dilution of 10x TBS stock) was added as a quencher for 5 minutes to each well. For permeabilization, 200-300 µL of a 0.1% Triton X-100 solution was added for 15 min. 200-300 µL of either 10% goat serum (Sigma-Aldrich, Catalog #G9023-10ML) in 1xTBS **or** 10% donkey serum (Sigma-Aldrich, Catalog #D9663-10ML) in 1xTBS blocking solution was added for either i) 1 h at room temperature **or** ii) overnight at 4° in a humidity cassette. Both primary and secondary antibodies were diluted in blocking solutions. 100-200 µL of 1:200 HDAC6 (Cell Signaling Technology, Catalog #7558S) antibody was added and left to incubate overnight at 4°C in a humidity cassette. All wells were washed three times with an appropriate volume of 1xTBS for a total of 15 min between stainings. 100-200 µL of secondary antibody (AlexaFluor, ThermoFischer) was added for 1-1.5 h at room temperature, protected from light. A 300 nM solution of DAPI (hydrochloride) (StemCell Technologies, Germany, Catalog #75004) was prepared from an 8 µM

stock and added for 5 min, followed by a single 1xTBS wash. After removing buffer from all wells, the chamber slide cover was removed and 1-2 drops of ProLong Gold Antifade reagent (Invitrogen, Catalog #P36934) were added to each well. Finally, a rectangular coverslip (24x50 mm, Menzel-Glaeser) was carefully placed on-top. All samples were left to mount at 4 °C overnight.

Widefield Microscopy:

All samples were imaged using a Zeiss Axioobserver.Z1/7 wide field microscope.

Aquisition Settings:

Objective EC Plan-Neofluar 40x/1.30 oil. Filters 335-383, 420-470, 550-580, 690-650

Track 1 DAPI, Beamsplitter (395), Excitation 353 nm, Emission 465 nm, Light Source (HXP 120V), Lamp Intensity (24.95%), Exposure 18.47 ms

Track 2 Alexa Fluor 568, Beamsplitter (585), Excitation 280 nm, Emission 618 nm, Light Source (HXP 120BV), Lamp Intensity (87.55%), Exposure 700 ms

Sensor Resolution 4096x3008 pixels

PAINS analysis

We filtered all compounds for pan-assay interference compounds (PAINS) using the online filter http://zinc15.docking.org/patterns/home/.[59] No compound was flagged as PAINS.

AUTHOR INFORMATION

Corresponding Author

F.K.H.: phone, (+49) 228 73 5213; fax, (+49) 228 73 7929; E-mail, finn.hansen@uni-bonn.de.

S.B.: phone, (+49) 211 81 04896; fax, (+49) 211 81 16436; E-mail, sanil.bhatia@med.uni-duesseldorf.de.

ORCID

Finn K. Hansen: 0000-0001-9765-5975

Sanil Bhatia: 0000-0001-6494-7744

Laura Sinatra: 0000-0002-2467-3803

Jing Yang: 0000-0002-7567-3176

Julian Schliehe-Diecks: 0000-0002-7166-4950

Author Contributions

L.S. and J.Y. share the first authorship. S.B. and F.K.H. contributed equally to this work as senior authors. The manuscript was written through contributions of all authors. All authors have given approval to the final version.

Notes

The authors declare no competing financial interest.

ACKNOWLEDGMENTS

S.B. acknowledges the financial support by Düsseldorf School of Oncology-Netzwerkverbundes and Forschungskommission (2018-04) HHU Düsseldorf. This study is funded in part by KinderKrebsForschung e.V. and the Deutsche Forschungsgemeinschaft (DFG, German Research Foundation) – 270650915 (Research Training Group GRK 2158, TP2d to S.B.). A.B. is supported by the TransOnc priority program of the German Cancer Aid within grant #70112951 (ENABLE). A.B. additionally acknowledges the financial support from Katharina-Hardt Foundation, Christiane und Claudia Hempel-foundation and especially Löwenstern e.V. for funding Simple Western system (JESS). Experimental support from Jannik Knoche is gratefully aknowledged.

ABBREVIATIONS

$CDCl_3$, chloroform-*d*; DMSO, dimethylsulfoxide; DCM, dichloromethane; Et_2O, diethyl ether**;** EtOAc, ethyl acetate; MeOH, methanol; min, minutes; petrol, petroleum ether; PROTAC, proteolysis targeting chimera, rt, room temperature; TFA, trifluoroacetic acid

REFERENCES

(1) Neklesa, T. K.; Winkler, J. D.; Crews, C. M. Targeted Protein Degradation by PROTACs. *Pharmacol. Ther.* **2017**, *174*, 138–144.

(2) Paiva, S.-L.; Crews, C. M. Targeted Protein Degradation: Elements of PROTAC Design. *Curr. Opin. Chem. Biol.* **2019**, *50*, 111–119.

(3) Nalawansha, D. A.; Crews, C. M. PROTACs: An Emerging Therapeutic Modality in Precision Medicine. *Cell Chem. Biol.* **2020**, *27*, 998–1014.

(4) Ishida, T.; Ciulli, A. E3 Ligase Ligands for PROTACs: How They Were Found and How to Discover New Ones. *SLAS Discov.* **2020**.

(5) Liu, J.; Chen, H.; Xie, L.; Chen, X.; Jin, J.; Wei, W. TF-PROTACs Enable Targeted Degradation of Transcription Factors. **2021**.

(6) Zheng, M.; Huo, J.; Gu, X.; Wang, Y.; Wu, C.; Zhang, Q.; Wang, W.; Liu, Y.; Liu, Y.; Zhou, X.; Chen, L.; Zhou, Y.; Li, H. Rational Design and Synthesis of Novel Dual PROTACs for Simultaneous Degradation of EGFR and PARP. *J. Med. Chem.* **2021**.

(7) https://clinicaltrials.gov/ trial numbers NCT03888612 and NCT04072952.

(8) Nalawansha, D. A.; Crews, C. M. PROTACs: An Emerging Therapeutic Modality in Precision Medicine. *Cell Chem. Biol.* **2020**, *27*, 998–1014.

(9) Mullard, A. Targeted Protein Degraders Crowd into the Clinic. *Nat. Rev. Drug Discov.* **2021**, *20*, 247–250.

(10) Strahl, B. D.; Allis, C. D. The Language of Covalent Histone Modifications. *Nature* **2000**, *403*, 41–45.

(11) Bolden, J. E.; Peart, M. J.; Johnstone, R. W. Anticancer Activities of Histone Deacetylase Inhibitors. *Nat. Rev. Drug Discov.* **2006**, *5*, 769–784.

(12) Park, S. Y.; Kim, J. S. A Short Guide to Histone Deacetylases Including Recent Progress on Class II Enzymes. *Exp. Mol. Med.* **2020**, *52*, 204–212.

(13) Hsu, K. C.; Liu, C. Y.; Lin, T. E.; Hsieh, J. H.; Sung, T. Y.; Tseng, H. J.; Yang, J. M.; Huang, W. J. Novel Class IIa-Selective Histone Deacetylase Inhibitors Discovered Using an in Silico

Virtual Screening Approach. *Sci. Rep.* **2017**, *7*, 1–13.

(14) Xiao, Y.; Wang, J.; Zhao, L. Y.; Chen, X.; Zheng, G.; Zhang, X.; Liao, D. Discovery of Histone Deacetylase 3 (HDAC3)-Specific PROTACs. *Chem. Commun.* **2020**, *56*, 9866–9869.

(15) Glozak, M. A.; Seto, E. Histone Deacetylases and Cancer. *Oncogene* **2007**, *26*, 5420–5432.

(16) Wang, P.; Wang, Z.; Liu, J. Role of HDACs in Normal and Malignant Hematopoiesis. *Mol. Cancer* **2020**, *19*, 1–21.

(17) Ropero, S.; Esteller, M. The Role of Histone Deacetylases (HDACs) in Human Cancer. *Mol. Oncol.* **2007**, *1*, 19–25.

(18) Li, Y.; Seto, E. HDACs and HDAC Inhibitors in CancerDevelopment and Therapy. *Cold Spring Harb Perspect Med* **2016**, 6:a026831.

(19) Clawson, G. A. Histone Deacetylase Inhibitors as Cancer Therapeutics. *Ann. Transl. Med.* **2016**, *4*, 1–5.

(20) Yang, K.; Wu, H.; Zhang, Z.; Leisten, E. D.; Nie, X.; Liu, B.; Wen, Z.; Zhang, J.; Cunningham, M. D.; Tang, W. Development of Selective Histone Deacetylase 6 (HDAC6) Degraders Recruiting von Hippel-Lindau (VHL) E3 Ubiquitin Ligase. *ACS Med. Chem. Lett.* **2020**, *11*, 575–581.

(21) Osko, J. D.; Christianson, D. W. Structural Basis of Catalysis and Inhibition of HDAC6 CD1, the Enigmatic Catalytic Domain of Histone Deacetylase 6. *Biochemistry* **2019**, *58*, 4912–4924.

(22) Schiedel, M.; Herp, D.; Hammelmann, S.; Swyter, S.; Lehotzky, A.; Robaa, D.; Oláh, J.; Ovádi, J.; Sippl, W.; Jung, M. Chemically Induced Degradation of Sirtuin 2 (Sirt2) by a Proteolysis Targeting Chimera (PROTAC) Based on Sirtuin Rearranging Ligands (SirReals). *J. Med. Chem.* **2018**, *61*, 482–491.

(23) Yang, K.; Song, Y.; Xie, H.; Wu, H.; Wu, Y.-T.; Leisten, E. D.; Tang, W. Development of the First Small Molecule Histone Deacetylase 6 (HDAC6) Degraders. *Bioorg. Med. Chem. Lett.* **2018**, *28*, 2493–2497.

(24) Xiao, Y.; Wang, J.; Zhao, L. Y.; Chen, X.; Zheng, G.; Zhang, X.; Liao, D. Discovery of Histone Deacetylase 3 (HDAC3)-Specific PROTACs. *Chem. Commun.* **2020**, *56*, 9866–9869.

(25) Lu, Y.; Sun, D.; Xiao, D.; Shao, Y.; Su, M.; Zhou, Y.; Li, J.; Zhu, S.; Lu, W. Design, Synthesis, and Biological Evaluation of HDAC Degraders with CRBN E3 Ligase Ligands. *Molecules* **2021**, *26*, 7241.

(26) Xiong, Y.; Donovan, K. A.; Eleuteri, N. A.; Kirmani, N.; Yue, H.; Razov, A.; Krupnick, N. M.; Nowak, R. P.; Fischer, E. S. Chemo-Proteomics Exploration of HDAC Degradability by Small Molecule Degraders. *Cell Chem. Biol.* **2021**, *28*, 1514-1527.e4.

(27) Chotitumnavee, J.; Yamashita, Y.; Takahashi, Y.; Takada, Y.; Iida, T.; Oba, M.; Itoh, Y.; Suzuki, T. Selective Degradation of Histone Deacetylase 8 Mediated by a Proteolysis Targeting Chimera (PROTAC). *Chem. Commun.* **2022**, *58*, 4635–4638.

(28) Smalley, J. P.; Baker, I. M.; Pytel, W. A.; Lin, L.-Y.; Bowman, K. J.; Schwabe, J. W. R.; Cowley, S. M.; Hodgkinson, J. T. Optimization of Class I Histone Deacetylase PROTACs Reveals That HDAC1/2 Degradation Is Critical to Induce Apoptosis and Cell Arrest in Cancer Cells. *J. Med. Chem.* **2022**, *65*, 5642–5659.

(29) Sun, Z.; Deng, B.; Yang, Z.; Mai, R.; Huang, J.; Ma, Z.; Chen, T.; Chen, J. Discovery of Pomalidomide-Based PROTACs for Selective Degradation of Histone Deacetylase 8. *Eur. J. Med. Chem.* **2022**, *239*, 114544.

(30) Yang, H.; Lv, W.; He, M.; Deng, H.; Li, H.; Wu, W.; Rao, Y. Plasticity in Designing PROTACs for Selective and Potent Degradation of HDAC6. *Chem. Commun.* **2019**, *55*, 14848–14851.

(31) Wu, H.; Yang, K.; Zhang, Z.; Leisten, E. D.; Li, Z.; Xie, H.; Liu, J.; Smith, K. A.; Novakova, Z.; Barinka, C.; Tang, W. Development of Multifunctional Histone Deacetylase 6 Degraders with Potent Antimyeloma Activity. *J. Med. Chem.* **2019**, *62*, 7042–7057.

(32) An, Z.; Lv, W.; Su, S.; Wu, W.; Rao, Y. Developing Potent PROTACs Tools for Selective Degradation of HDAC6 Protein. *Protein Cell* **2019**, *10*, 606–609.

(33) Yang, K.; Zhao, Y.; Nie, X.; Wu, H.; Wang, B.; Almodovar-Rivera, C. M.; Xie, H.; Tang, W. A Cell-Based Target Engagement Assay for the Identification of Cereblon E3 Ubiquitin Ligase Ligands and Their Application in HDAC6 Degraders. *Cell Chem. Biol.* **2020**, *27*, 866-876.e8.

(34) Sinatra, L.; Bandolik, J. J.; Roatsch, M.; Sönnichsen, M.; Schoeder, C. T.; Hamacher, A.; Schöler, A.; Borkhardt, A.; Meiler, J.; Bhatia, S.; Kassack, M. U.; Hansen, F. K. Hydroxamic

Acids Immobilized on Resins (HAIRs): Synthesis of Dual-Targeting HDAC Inhibitors and HDAC Degraders (PROTACs). *Angew. Chem. Int. Ed.* **2020**, *59*, 22494–22499.

(35) Yang, K.; Wu, H.; Zhang, Z.; Leisten, E. D.; Nie, X.; Liu, B.; Wen, Z.; Zhang, J.; Cunningham, M. D.; Tang, W. Development of Selective Histone Deacetylase 6 (HDAC6) Degraders Recruiting Von Hippel–Lindau (VHL) E3 Ubiquitin Ligase. *ACS Med. Chem. Lett.* **2020**, *11*, 575–581.

(36) Smalley, J. P.; Adams, G. E.; Millard, C. J.; Song, Y.; Norris, J. K. S.; Schwabe, J. W. R.; Cowley, S. M.; Hodgkinson, J. T. PROTAC-Mediated Degradation of Class I Histone Deacetylase Enzymes in Corepressor Complexes. *Chem. Commun.* **2020**, *56*, 4476–4479.

(37) Cao, F.; de Weerd, S.; Chen, D.; Zwinderman, M. R. H.; van der Wouden, P. E.; Dekker, F. J. Induced Protein Degradation of Histone Deacetylases 3 (HDAC3) by Proteolysis Targeting Chimera (PROTAC). *Eur. J. Med. Chem.* **2020**, *208*, 112800.

(38) Keuler, T.; König, B.; Bückreiß, N.; Kraft, F. B.; König, P.; Schäker-Hübner, L.; Steinebach, C.; Bendas, G.; Gütschow, M.; Hansen, F. K. Development of the First Non-Hydroxamate Selective HDAC6 Degraders. *Chem. Commun.* **2022**, *58*, 11087–11090.

(39) Macabuag, N.; Esmieu, W.; Breccia, P.; Jarvis, R.; Blackaby, W.; Lazari, O.; Urbonas, L.; Eznarriaga, M.; Williams, R.; Strijbosch, A.; Van de Bospoort, R.; Matthews, K.; Clissold, C.; Ladduwahetty, T.; Vater, H.; Heaphy, P.; Stafford, D. G.; Wang, H.; Mangette, J. E.; McAllister, G.; Beaumont, V.; Vogt, T. F.; Wilkinson, H. A.; Doherty, E. M.; Dominguez, C. Developing HDAC4-Selective Protein Degraders To Investigate the Role of HDAC4 in Huntington's Disease Pathology. *J. Med. Chem.* **2022**, *65*, 12445–12459.

(40) Darwish, S.; Ghazy, E.; Heimburg, T.; Herp, D.; Zeyen, P.; Salem-Altintas, R.; Ridinger, J.; Robaa, D.; Schmidtkunz, K.; Erdmann, F.; Schmidt, M.; Romier, C.; Jung, M.; Oehme, I.; Sippl, W. Design, Synthesis and Biological Characterization of Histone Deacetylase 8 (HDAC8) Proteolysis Targeting Chimeras (PROTACs) with Anti-Neuroblastoma Activity. *Int. J. Mol. Sci.* **2022**, *23*, 7535.

(41) Paiva, S. L.; Crews, C. M. Targeted Protein Degradation: Elements of PROTAC Design. *Curr. Opin. Chem. Biol.* **2019**, *50*, 111–119.

(42) Shen, S.; Benoy, V.; Bergman, J. A.; Kalin, J. H.; Frojuello, M.; Vistoli, G.; Haeck, W.; Van Den Bosch, L.; Kozikowski, A. P. Bicyclic-Capped Histone Deacetylase 6 Inhibitors with Improved Activity in a Model of Axonal Charcot-Marie-Tooth Disease. *ACS Chem. Neurosci.* **2016**, *7*, 240–258.

(43) Sinatra, L.; Bandolik, J. J.; Roatsch, M.; Sönnichsen, M.; Schoeder, C. T.; Hamacher, A.; Schöler, A.; Borkhardt, A.; Meiler, J.; Bhatia, S.; Kassack, M. U.; Hansen, F. K. Hydroxamic Acids Immobilized on Resins (HAIRs): Synthesis of Dual-Targeting HDAC Inhibitors and HDAC Degraders (PROTACs). *Angew. Chem. Int. Ed.* **2020**, *59*, 22494–22499.

(44) Lohbeck, J.; Miller, A. K. Practical Synthesis of a Phthalimide-Based Cereblon Ligand to Enable PROTAC Development. *Bioorg. Med. Chem. Lett.* **2016**, *26*, 5260–5262.

(45) Steinebach, C.; Kehm, H.; Lindner, S.; Vu, L. P.; Köpff, S.; López Mármol, Á.; Weiler, C.; Wagner, K. G.; Reichenzeller, M.; Krönke, J.; Gütschow, M. PROTAC-Mediated Crosstalk between E3 Ligases. *Chem. Commun.* **2019**, *55*, 1821–1824.

(46) Wu, H.; Yang, K.; Zhang, Z.; Leisten, E. D.; Li, Z.; Xie, H.; Liu, J.; Smith, K. A.; Novakova, Z.; Barinka, C.; Tang, W. Development of Multifunctional Histone Deacetylase 6 Degraders with Potent Antimyeloma Activity. *J. Med. Chem.* **2019**, *62*, 7042–7057.

(47) Schwinn, M. K.; Steffen, L. S.; Zimmerman, K.; Wood, K. V.; Machleidt, T. A Simple and Scalable Strategy for Analysis of Endogenous Protein Dynamics. *Sci. Rep.* **2020**, *10*, 8953.

(48) Depetter, Y.; Geurs, S.; De Vreese, R.; Goethals, S.; Vandoorn, E.; Laevens, A.; Steenbrugge, J.; Meyer, E.; de Tullio, P.; Bracke, M.; D'hooghe, M.; De Wever, O. Selective Pharmacological Inhibitors of HDAC6 Reveal Biochemical Activity but Functional Tolerance in Cancer Models. *Int. J. Cancer* **2019**, *145*, 735–747.

(49) Reßing, N.; Sönnichsen, M.; Osko, J. D.; Schöler, A.; Schliehe-Diecks, J.; Skerhut, A.; Borkhardt, A.; Hauer, J.; Kassack, M. U.; Christianson, D. W.; Bhatia, S.; Hansen, F. K. Multicomponent Synthesis, Binding Mode, and Structure–Activity Relationship of Selective Histone Deacetylase 6 (HDAC6) Inhibitors with Bifurcated Capping Groups. *J. Med. Chem.* **2020**, *63*, 10339–10351.

(50) Yang, C.-J.; Liu, Y.-P.; Dai, H.-Y.; Shiue, Y.-L.; Tsai, C.-J.; Huang, M.-S.; Yeh, Y.-T. Nuclear

HDAC6 Inhibits Invasion by Suppressing NF-KB/MMP2 and Is Inversely Correlated with Metastasis of Non-Small Cell Lung Cancer. *Oncotarget* **2015**, *6*, 30263–30276.

(51) Yang, D.; Fu, H.; Hu, L.; Jiang, Y.; Zhao, Y. Copper-Catalyzed Synthesis of Benzimidazoles via Cascade Reactions of o-Haloacetanilide Derivatives with Amidine Hydrochlorides. *J. Org. Chem.* **2008**, *73*, 7841–7844.

(52) Álvarez, S.; Khanwalkar, H.; Álvarez, R.; Erb, C.; Martínez, C.; Rodríguez-Barrios, F.; Germain, P.; Gronemeyer, H.; de Lera, A. R. C3 Halogen and C8″ Substituents on Stilbene Arotinoids Modulate Retinoic Acid Receptor Subtype Function. *ChemMedChem* **2009**, *4*, 1630–1640.

(53) Galoppini, C.; Meini, S.; Tancredi, M.; Di Fenza, A.; Triolo, A.; Quartara, L.; Maggi, C. A.; Formaggio, F.; Toniolo, C.; Mazzucco, S.; Papini, A.; Rovero, P. A New Class of Pseudopeptide Antagonists of the Kinin B 1 Receptor Containing Alkyl Spacers. *J. Med. Chem.* **1999**, *42*, 409–414.

(54) Steinebach, C.; Kehm, H.; Lindner, S.; Vu, L. P.; Köpff, S.; López Mármol, Á.; Weiler, C.; Wagner, K. G.; Reichenzeller, M.; Krönke, J.; Gütschow, M. PROTAC-Mediated Crosstalk between E3 Ligases. *Chem. Commun.* **2019**, *55*, 1821–1824.

(55) Erdeljac, N.; Bussmann, K.; Schöler, A.; Hansen, F. K.; Gilmour, R. Fluorinated Analogues of the Histone Deacetylase Inhibitor Vorinostat (Zolinza): Validation of a Chiral Hybrid Bioisostere, BITE. *ACS Med. Chem. Lett.* **2019**, *10*, 1336–1340.

(56) Poschmann, G.; Seyfarth, K.; Besong Agbo, D.; Klafki, H.-W.; Rozman, J.; Wurst, W.; Wiltfang, J.; Meyer, H. E.; Klingenspor, M.; Stühler, K. High-Fat Diet Induced Isoform Changes of the Parkinson's Disease Protein DJ-1. *J. Proteome Res.* **2014**, *13*, 2339–2351.

(57) Hughes, C. S.; Moggridge, S.; Müller, T.; Sorensen, P. H.; Morin, G. B.; Krijgsveld, J. Single-Pot, Solid-Phase-Enhanced Sample Preparation for Proteomics Experiments. *Nat. Protoc.* **2019**, *14*, 68–85.

(58) Tusher, V. G.; Tibshirani, R.; Chu, G. Significance Analysis of Microarrays Applied to the Ionizing Radiation Response. *Proc. Natl. Acad. Sci. U.S.A.* **2001**, *98*, 5116–5121.

(59) Baell, J. B.; Holloway, G. A. New Substructure Filters for Removal of Pan Assay Interference Compounds (PAINS) from Screening Libraries and for Their Exclusion in Bioassays. *J. Med.*

Chem. **2010**, *53*, 2719–2740.